



HAL
open science

Experimental screening of metal nitrides hydrolysis for green ammonia synthesis via solar thermochemical looping

Stéphane Abanades, Bertrand Rebiere, Martin Drobek, Anne Julbe

► To cite this version:

Stéphane Abanades, Bertrand Rebiere, Martin Drobek, Anne Julbe. Experimental screening of metal nitrides hydrolysis for green ammonia synthesis via solar thermochemical looping. *Chemical Engineering Science*, 2024, 283, pp.119406. 10.1016/j.ces.2023.119406 . hal-04251780

HAL Id: hal-04251780

<https://hal.science/hal-04251780>

Submitted on 20 Oct 2023

HAL is a multi-disciplinary open access archive for the deposit and dissemination of scientific research documents, whether they are published or not. The documents may come from teaching and research institutions in France or abroad, or from public or private research centers.

L'archive ouverte pluridisciplinaire **HAL**, est destinée au dépôt et à la diffusion de documents scientifiques de niveau recherche, publiés ou non, émanant des établissements d'enseignement et de recherche français ou étrangers, des laboratoires publics ou privés.

Experimental screening of metal nitrides hydrolysis for green ammonia synthesis via solar thermochemical looping

Stéphane Abanades^{1*}, Bertrand Rebiere², Martin Drobek², Anne Julbe²

¹ CNRS; Processes, Materials and Solar Energy laboratory (PROMES); 7 rue du Four Solaire; 66120 Odeillo Font-Romeu; France

² Institut Européen des Membranes (IEM); CNRS, ENSCM, Univ Montpellier; Place Eugène Bataillon; 34095 Montpellier; France

* Corresponding author: stephane.abanades@promes.cnrs.fr

Abstract

Ammonia is a fundamental chemical commodity for fertilizer and as a novel energy vector. Solar-driven ammonia synthesis is proposed as a sustainable alternative to the catalytic energy-intensive and CO₂-emitting Haber-Bosch process. The considered thermochemical process aims to produce ammonia from nitrogen and water ($N_2+3H_2O\rightarrow 2NH_3+1.5O_2$) via redox cycles using a solar heat source, thus bypassing the supply of H₂ or electricity. Metal oxide/nitride redox pairs can be employed for this cyclic process. The exothermal hydrolysis reaction of nitrides produces ammonia ($M_xN_y+3H_2O\rightarrow 2NH_3+M_xO_y$), and is followed by one or several regeneration steps ($M_xO_y+N_2\rightarrow M_xN_y+3/2O_2$) requiring a heat supply from concentrated solar energy. This study aims to experimentally identify the most suitable metal nitrides in the hydrolysis step for ammonia synthesis based on solar-driven chemical-looping. As a result, FeN, CrN, BN, and Si₃N₄ turned out to be irrelevant candidates for NH₃ production, as the hydrolysis yield was poor up to 1000°C. In contrast, AlN, Li₃N, Ca₃N₂, Mg₃N₂, TiN, and ZrN exhibited noteworthy reactivity depending on the temperature. The hydrolysis rate of AlN was significantly enhanced only above 1100°C, TiN showed an increasing NH₃ production rate with temperature (reaching 3.4 mmol/min/g at 1000°C), while an optimum at 750°C was unveiled for complete ZrN conversion (corresponding to the highest rate of 34.2 mmol/min/g). Hydrolysis of Li₃N, Ca₃N₂, and Mg₃N₂ was complete at lower temperatures (~200°C), with NH₃ yields of 5.9, 4.9, and 18.6 mmol/g, respectively. Solar-driven regeneration of metal nitrides at high temperature will be then necessary to demonstrate the complete feasibility of thermochemical cycles for green ammonia synthesis.

Keywords: ammonia synthesis, solar fuel, metal nitrides, chemical-looping, thermochemical cycles, hydrogen carrier.

1. Introduction

Ammonia is one of the most produced industrial chemical compounds with a current production of 168.1 million tons and annual growth of more than 2% to reach 197.2 million tons in 2026 (Mordor Intelligence LLP, 2021). Ammonia is a fundamental component of ammonium nitrate fertilizer. Hence, the main application sector is that of fertilizers for agriculture, while new applications as an energy carrier or as an effective means of hydrogen storage (Aziz et al., 2020) show a growing interest in proposing alternatives to fossil fuels. An increasing demand in ammonia is thus foreseen in the future. Ammonia as a clean fuel (and hydrogen carrier/vector) is promising since it can be stored more easily than hydrogen in the liquid form (NH₃ boiling point = -33.4 °C at 1 atm versus -253 °C for H₂) and it offers a higher volumetric energy density (12.7 MJ/L) than liquid hydrogen (8.5 MJ/L). Furthermore, vast ammonia infrastructure already exists due to its extensive use for fertilizers.

The search for carbon-free alternatives and less energy-intensive solutions for NH₃ production represents a major challenge for the years to come. Indeed, ammonia is currently produced by the Haber-Bosch process ($N_{2(g)} + 3H_{2(g)} \rightleftharpoons 2NH_{3(g)}$, $\Delta H^\circ = -91.9 \text{ kJ mol}^{-1}$) developed more than a century ago, which is highly energy-intensive and generates greenhouse gas (GHG) emissions (2.2 tons CO₂ / ton NH₃ (Rafiqul et al., 2005)). The ammonia production represents about 2% of the world consumption of fossil energy and generates over 420 million tons of

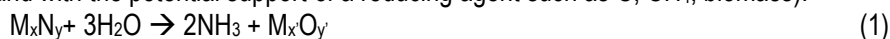
54 CO₂ per year, thus representing 1.2% of global anthropic CO₂ emissions (Liu et al., 2020). The Haber-Bosch
55 process consists in reacting hydrogen (H₂) with nitrogen (N₂) using catalysts at high temperatures and pressures
56 (400/650°C – 200/400 bars) and relies on fossil fuels. Indeed, the hydrogen required for the synthesis of ammonia
57 is currently produced by steam reforming of natural gas, while N₂ is obtained by cryogenic separation of air. Both
58 of these processes require a large input of energy, causing significant concomitant GHG emissions. Specific studies
59 have been proposed to improve the efficiency of NH₃ synthesis unit by associating a tri-reforming reactor with a
60 membrane unit (Damanabi et al., 2019). However, the use of ammonia as an energy carrier cannot be considered
61 as a decarbonized source when using hydrogen of fossil origin. It is thus necessary to develop alternatives to the
62 Haber-Bosch process. In order to make ammonia a sustainable energy carrier in the future, the decarbonation of
63 its production and the use of a renewable energy source are necessary. The decarbonation of ammonia production
64 can be achieved by using green hydrogen (produced by electrolysis) or by directly producing ammonia via new
65 electrochemical or thermochemical processes. However, with the increasing deployment of hydrogen as an energy
66 carrier in the transport sector or for industrial applications (e.g., for direct reduced iron and steel metallurgy (Bhaskar
67 et al., 2020; Patisson and Mirgoux, 2020)), it becomes necessary to develop alternatives for ammonia production
68 in order to avoid consuming the green hydrogen feedstocks that will be produced. The direct use of H₂ in the
69 process should therefore be avoided, while preferring production from nitrogen and water.

70
71 To avoid using the Haber-Bosch process, the synthesis of ammonia from renewable energies must be developed
72 on an industrial scale (Wang et al., 2018). Accordingly, the primary energy source can be used either in the form
73 of electricity or in the form of heat. The solar-driven production of ammonia by directly using the heat generated by
74 solar concentrating systems with a higher energy conversion efficiency than electrolysis (because it is not limited
75 by the efficiency of the intermediate electricity production) appears to be an ideal solution (Abanades, 2023). This
76 method is advantageous because it can potentially produce ammonia from N₂ and H₂O without electricity input or
77 hydrogen consumption. The overall reaction is however highly endothermic ($N_2 + 3H_2O \rightarrow 2NH_3 + \frac{3}{2}O_2$, $\Delta H^\circ =$
78 633.6 kJ/mol), it cannot occur spontaneously due to the high stability of nitrogen and requires a significant energy
79 input (either heat or electricity). Therefore, the use of concentrated solar energy for providing the reaction enthalpy
80 represents a major interest. This reaction corresponds to the reverse of NH₃ combustion, achievable thanks to
81 contribution of solar energy.

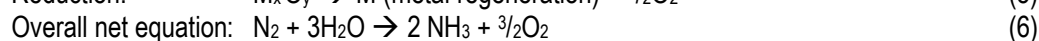
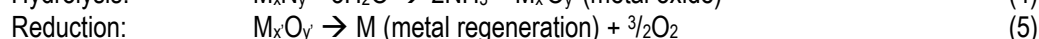
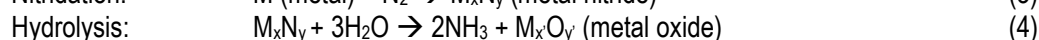
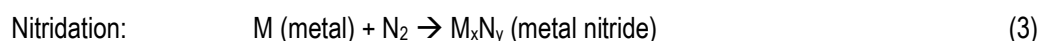
82
83 Various alternative methods of ammonia production under mild conditions have been proposed, especially for solar
84 energy integration in low-pressure green ammonia production technologies (Klaas et al., 2021). Possible processes
85 include solid state synthesis, molten salt synthesis, thermochemical looping and photocatalytic routes.
86 Electrochemical processes based on green electricity produced by renewable energies have been studied to
87 synthesize ammonia, among which one can cite solid-state ammonia synthesis (SSAS) (Kishira et al., 2017;
88 Kyriakou et al., 2017; Marnellos et al., 2000; Marnellos and Stoukides, 1998; Qing et al., 2016) or synthesis by
89 means of molten salts (Murakami et al., 2005a, 2005b, 2003). Such electrochemical processes require electrodes
90 and an electrolyte (solid or molten salts) and have the advantage of not requiring high pressures. However, in some
91 electrochemical processes, the synthesis still makes use of N₂ and H₂, it is thus necessary to privilege the processes
92 rather based on the use of N₂ and water. Among the main drawbacks of such processes, it can be noticed that the
93 electrodes generally include noble metals (Pd, Pt, Ru) (Ceballos et al., 2021), the NH₃ production rates are low,
94 and the overall efficiency of the process remains limited by the conversion of the primary energy source into
95 electricity. Other routes have considered the chemical looping of metal nitrides consisting of a reduction of N₂ with
96 a looped metal nitride ($M_aN_{b-\delta} + \delta/2 N_2 \rightarrow M_aN_b$), followed by separate hydrogenation of the lattice nitrogen in
97 ammonia ($M_aN_b + 3\delta/2 H_2 \rightarrow M_aN_{b-\delta} + \delta NH_3$) (Daisley and Hargreaves, 2023; Goto et al., 2021; Hunter et al., 2010;
98 Laassiri et al., 2018; Michalsky et al., 2015a; Yang et al., 2022). However, such a process still relies on the use of
99 H₂ as feedstock, since the net reaction remains unchanged ($N_2 + 3H_2 \rightarrow 2NH_3$), and the exothermicity of this global
100 reaction makes the use of solar energy less attractive.

101
102 As an alternative to the Haber-Bosch process and the electrochemical synthesis of ammonia, this study aims to
103 develop thermochemical processes for the production of ammonia from N₂ and H₂O, using concentrated solar
104 energy as a high-temperature heat source. Previous works have already been devoted to the development of solar-
105 driven thermochemical redox cycles for water splitting to produce hydrogen (Abanades, 2022; Haeussler et al.,
106 2019; Le Gal and Abanades, 2011; Xiao et al., 2012). Reduction of metal oxides using high-temperature solar heat
107 has also been proved to be feasible (Chambon et al., 2010a, 2010b; Chuayboon and Abanades, 2019). Similarly,
108 metal oxide/nitride redox cycles can be proposed. Chemical-looping ammonia production pathways have been

109 reviewed (Lai et al., 2022). The ammonia synthesis reaction from water and nitrogen can be decomposed into
110 several steps, with high-temperature heat supplied by concentrated solar radiation as the only energy input. Such
111 cycles for solar thermochemical ammonia production can be operated in two or three steps, using different reactive
112 intermediate materials participating in the reactions. This makes possible the ammonia synthesis under milder
113 conditions (atmospheric pressure and temperatures compatible with concentrated solar energy). For instance, two-
114 step cycles involve a reaction of metal nitride with water vapour to produce ammonia and the metal oxide (Eq. 1),
115 followed by an endothermic step (Eq. 2) corresponding to the regeneration of metal nitride from the nitridation
116 reaction of the oxide with N₂ (and with the potential support of a reducing agent such as C, CH₄, biomass).



119
120 A three-step cycle based on the metal oxide/nitride redox pair can also be considered with the same overall net
121 reaction (Klaas et al., 2021) (note that equations are not balanced as they depend on the redox pair involved):
122



127
128 The main advantages of such cycles include: (i) the absence of a fossil energy source allowing the decarbonation
129 of ammonia production, (ii) the use of hydrogen as a reactant is not required, (iii) the reaction carried out at
130 atmospheric pressure, (iv) the absence of expensive catalysts and material consumption as the reactive materials
131 are cycled, (iv) the direct use of solar energy as a process heat source without intermediate production of electricity,
132 thereby enhancing overall energy conversion efficiencies. Recent theoretical studies have identified possible
133 oxide/nitride redox couples (Bartel et al., 2019), but to date very few experimental studies have demonstrated the
134 feasibility of solar ammonia production by thermochemical cycles. Nitrides of chromium, aluminum, lithium,
135 molybdenum and manganese were previously proposed and studied experimentally (Gálvez et al., 2008; Jain et
136 al., 2017; Michalsky et al., 2015b; Michalsky and Pfromm, 2011). However, there is no available comprehensive
137 experimental study comparing the ability of various nitrides to produce ammonia. In addition, high-throughput
138 equilibrium analysis and computational screening were also performed for rapid identification of candidate materials
139 (Bartel et al., 2019; Michalsky and Steinfeld, 2017). Regarding the synthesis of nitrides (regeneration step), the
140 solar carbothermal reduction of metal oxides (Al₂O₃, SiO₂, TiO₂, and ZrO₂) in N₂ to produce nitrides was
141 demonstrated (Murray et al., 1995), which confirmed the feasibility of nitrides synthesis from their oxides at high
142 temperatures with the addition of a reducing agent. The economics and scale-up ability of the technology have
143 been assessed (Gálvez et al., 2007b; Michalsky et al., 2012).
144

145 Solar ammonia production via thermochemical cycles based on metal nitrides is a suitable means for the
146 decarbonation of the industrial process, reducing both its environmental impact and its energy/economic costs.
147 Several innovative aspects of this approach can be mentioned. The solar process considered for ammonia
148 production avoids the direct use of hydrogen as a feedstock, while being a green process without electricity supply.
149 The cycles are solely based on metal nitrides as intermediate compounds and on solar heat for NH₃ production
150 from N₂ and H₂O as the only feedstocks. The development of active metal nitride materials for the hydrolysis step
151 to synthesize NH₃ with high yields and the high-temperature solar-driven regeneration for the nitridation step are
152 the main challenges for process performance enhancement, paving the way to industrial applications.

153 In particular, the reactivity of nitrides during hydrolysis must first be demonstrated experimentally to identify suitable
154 candidates for solar ammonia synthesis. Experimental screening of metal nitrides hydrolysis has never been done
155 before. There is no study comparing the reactivity of different nitrides in the literature. In addition, their ability to
156 produce ammonia during hydrolysis must be quantified and suitable operating conditions must be identified for
157 each candidate material. In this study, a series of metal nitrides was thus selected for an experimental screening
158 of their reactivity towards the production of NH₃. The aim was to identify the most suitable metal nitrides in the
159 hydrolysis step to synthesize NH₃ with high yields and production rates. The reaction conversion, hydrolysis rate,
160 and ammonia production capacity were evaluated by investigating the direct reaction of nitride powders with steam
161 in a packed-bed reactor, and the influence of temperature was probed. Ammonia production was directly measured
162 and quantified via continuous evolved gas analysis. Active metal nitride candidates with their corresponding
163 performance for ammonia synthesis were identified.

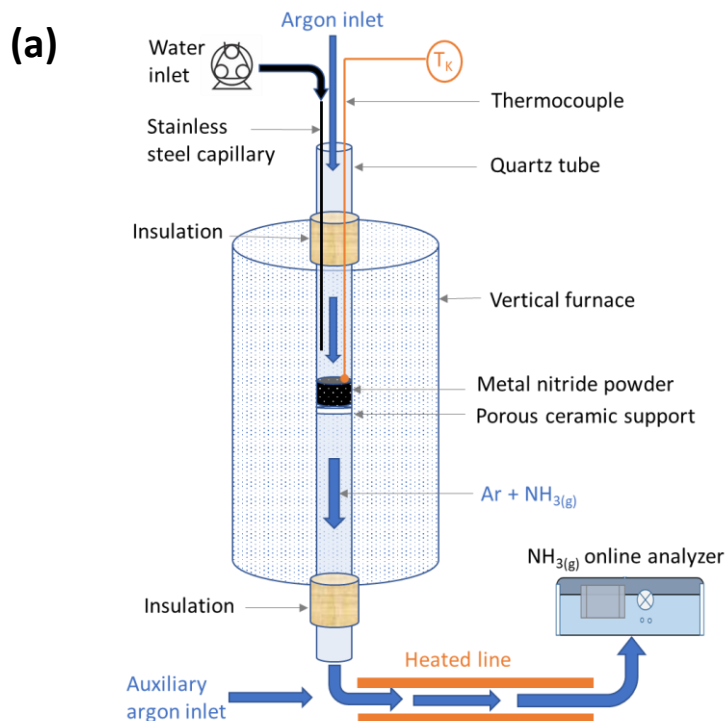
164
165
166
167
168
169
170
171
172
173
174
175
176
177
178
179
180
181
182
183
184
185
186
187
188
189

2. Experimental set-up and methods

2.1 Experimental bench

An experimental bench dedicated to the study of the hydrolysis step of metal nitrides with continuous evolved gas analysis has been specifically developed to perform nitrides screening and compare NH_3 production rates. The experimental set-up (Figure 1) is composed of a vertical tubular furnace to study the production of NH_3 at different temperatures. A tubular quartz reactor is placed inside the furnace. The metal nitride powder is loaded as a packed-bed ($\sim 0.1\text{-}0.5\text{ g}$) inside the vertical tubular furnace in the center of the quartz tube (16 mm inside diameter, middle of the tube 175 mm from the ends) and supported by a porous ceramic (zirconia felt).

The reactor is connected to a gas inlet to inject the carrier gas (Ar, 99.999% purity) with a flow-rate controlled by a mass-flow controller (MFC, Brooks, range 0-1 NL/min). A stainless-steel capillary is placed inside the quartz tube to inject water vapor using a calibrated peristaltic pump (for liquid water flow-rate control). The water is then vaporized as it flows through the capillary and exits as steam which is transported by the Ar carrier gas through the powder bed. At the quartz tube outlet, a heated line ($T > 120^\circ\text{C}$) is used to sample the exhaust gases towards an NH_3 analyzer, avoiding any condensation of steam in which the soluble NH_3 could be trapped. On this outlet, an auxiliary Ar input (MFC, Brooks, range 0-5 NL/min) is connected for the dilution of the NH_3 concentration in order to maintain it within the detection range of the analyzer. The maximum NH_3 concentration reached also depends on the initial mass of loaded nitride in the reactor, which must be thus controlled to avoid peak saturation. The exiting gas is analyzed using a dedicated UV-vis spectrophotometer (OMA-406, Applied Analytics, measurement cell heated to 150°C , range: 0-10000 ppm, calibrated with 5000 ppm NH_3 calibration gas) to continuously measure the ammonia concentration during hydrolysis and monitor the progress of the reaction (one measurement performed every 5 s). The reaction temperature is measured by a K-type thermocouple reaching inside the powder bed. Both the sample bed temperature and the NH_3 concentration are recorded continuously by data acquisition with a time step of 1 s.



190
191
192

(b)

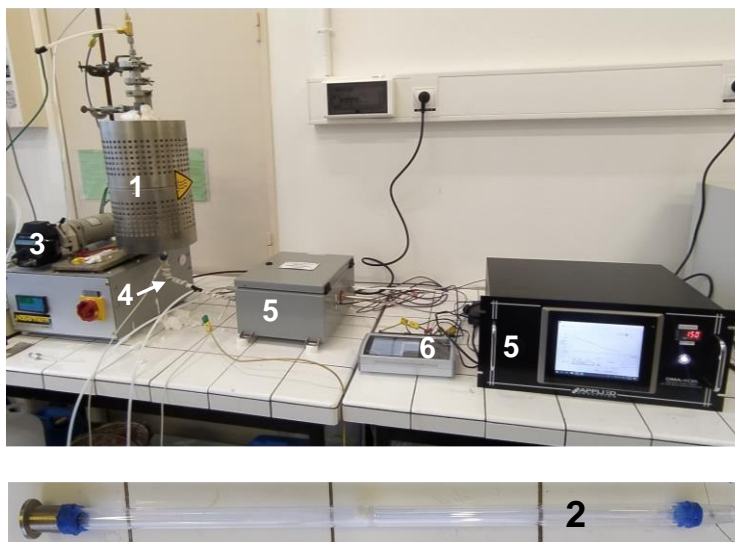
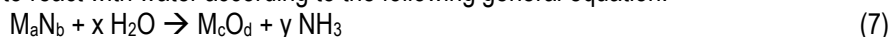


Figure 1. Experimental hydrolysis reactor and set-up: (a) Schematic of the packed-bed of commercial nitride powder in a vertical tubular furnace with continuous NH₃ analysis in the exit gas, (b) Photograph of the set-up (1. Tubular furnace; 2. Quartz tube reactor; 3. Peristaltic pump; 4. Heated line; 5. NH₃ analyzer; 6. Acquisition system).

2.2 Materials and methods

A series of ten commercial metal nitrides (Sigma Aldrich) was selected to investigate the hydrolysis reaction: AlN (purity $\geq 98\%$, metals basis), Li₃N (99.4%), Ca₃N₂ (99%), Mg₃N₂ (99.6%), TiN ($\geq 99.7\%$), CrN (Cr₂N+CrN, $\geq 99.5\%$), Fe_xN ($x=2-4$, $\geq 99.7\%$), BN ($\geq 99.7\%$), Si₃N₄ (99.9%), and ZrN (99.5%).

These materials are expected to react with water according to the following general equation:



Each material was thus tested during the hydrolysis reaction to compare the NH₃ production yields and the reaction rates at different temperatures.

The nitridation step was not studied in this work, but the carbothermal reduction of oxides in the presence of N₂ appears to be a favorable route for the regeneration of nitrides. For instance, the combined carbothermal reduction and nitridation of Al₂O₃, TiO₂, SiO₂ and ZrO₂ oxides are thermodynamically possible upon increasing temperature based on their Gibbs free enthalpy variation (Murray et al., 1995).

The experimental conditions are summarized in Table S1 (Supplementary Information). The Ar carrier gas flow-rate was set at 0.2 NL/min and the water vapor flow-rate was 0.224 NL/min. The resulting steam molar content in the reactor was therefore 52.8%. At the reactor outlet, the gas was diluted with Ar (typically 1.25 NL/min) before being injected into the analyzer to avoid saturation of the analysis cell and to remain within the suitable measurement range of the gas analysis system (0-10000 ppm). The nitride mass loaded in the reactor was thus maintained low enough to avoid excessively high ammonia concentrations in the outlet gas and to prevent signal saturation, thus warranting reliable online analysis. The amount of NH₃ evolved from the hydrolysis reactions was quantified, as detailed in the following. The NH₃ mole fraction (y_{NH_3}) was measured as a function of time. From these data, the production rate and the total amount of NH₃ can be calculated as follows:

$$Q_{NH_3} = \frac{y_{NH_3} \cdot Q_{total}}{m_{nitride}} \quad (8)$$

with Q_{NH_3} the NH₃ production rate per unit mass of nitride (mol.min⁻¹.g⁻¹), y_{NH_3} the NH₃ mole fraction at the reactor outlet, Q_{total} the total outlet gas molar flow-rate after dilution (mol/min), and $m_{nitride}$ the nitride mass loaded into the reactor (g).

Q_{total} depends on the studied nitride and the corresponding global reaction equation of the hydrolysis. Indeed, part of the injected steam is consumed during the reaction producing NH₃. The outlet gas flow-rate corresponds to the sum of the outlet flow-rates of argon (Q_{Ar}), unreacted steam ($Q_{H_2O,outlet}$) and NH₃, and is therefore expressed by:

231
232
$$Q_{\text{total}} = Q_{\text{Ar}} + Q_{\text{H}_2\text{O, outlet}} + m_{\text{nitride}} \cdot Q_{\text{NH}_3} \quad (9)$$

233
234 For example, in the case of Mg_3N_2 hydrolysis, the overall equation is given by:
235
$$\text{Mg}_3\text{N}_2 + 6 \text{H}_2\text{O} \rightarrow 3 \text{Mg}(\text{OH})_2 + 2 \text{NH}_3 \quad (10)$$

236

237 The flow-rate of unreacted steam can then be calculated as follows:
238
$$Q_{\text{H}_2\text{O, outlet}} = Q_{\text{H}_2\text{O, inlet}} - 3 \cdot Q_{\text{NH}_3} \quad (11)$$

239

240 By combining Eqs. (8), (9), and (11), Q_{NH_3} can be expressed as:
241
$$Q_{\text{NH}_3} = \frac{y_{\text{NH}_3} \cdot (Q_{\text{Ar}} + Q_{\text{H}_2\text{O, inlet}})}{(1 + 2y_{\text{NH}_3}) \cdot m_{\text{nitride}}} \quad (12)$$

242

243 The total amount of NH_3 produced (mol/g) is calculated by integrating the NH_3 molar flow-rate over the hydrolysis
244 step duration.

245
$$n_{\text{NH}_3} = \int_0^t Q_{\text{NH}_3} \cdot dt \quad (13)$$

246

247 The performance metrics including global amounts of generated ammonia and production rates were expressed
248 per unit mass of metal nitride (Eq. 8 and Eq. 13) for comparison purpose on the same basis.

249 The ammonia yield can then be obtained from:
250
$$X_{\text{NH}_3} = \frac{n_{\text{NH}_3}}{n_{\text{NH}_3, \text{max}}} \quad (14)$$

251

252 where $n_{\text{NH}_3, \text{max}}$ is the theoretical maximum amount of NH_3 calculated from the overall reaction equation.

253
254 In addition, the structure and microstructure of fresh and hydrolyzed materials were characterized by different
255 techniques to verify the powders conversion and to confirm that the reactions occur as expected.

256 Crystalline structure and phase identification were studied by X-ray diffraction (XRD) using a Panalytical X'PERT
257 PRO diffractometer with the Cu K α radiation ($\alpha_{\text{Cu}} = 0.15406 \text{ nm}$, angular range = $20\text{-}80^\circ$, 2θ , tube current 20 mA,
258 potential 40 kV).

259 The morphology of the materials was observed with a Field Emission Scanning Electron Microscope (FESEM -
260 Hitachi S4800) used to examine /compare the microstructure of the powders. An elemental chemical analysis
261 cartography was carried out by EDX analysis (Energy Dispersive X-ray Spectroscopy, using a Zeiss Sigma 300
262 with an accelerating voltage of 15 keV) to estimate the chemical composition and observe elements distribution
263 (surface mapping) in the materials.

264
265 In total, 44 hydrolysis runs were carried out with the experimental set-up in order to characterize the series of 10
266 metal nitrides considered (Table S1).

267 268 3. Results and discussion

269 270 3.1 Aluminum nitride (AlN)

271 The hydrolysis of AlN can be written:
272
$$2\text{AlN} + 3\text{H}_2\text{O} \rightarrow \text{Al}_2\text{O}_3 + 2\text{NH}_3 \quad \Delta H^\circ = -274.1 \text{ kJ/mol} \quad (15)$$

273

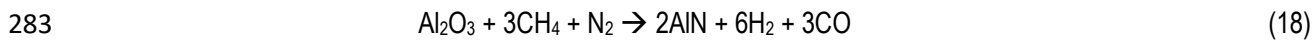
274 The theoretical production corresponds to one mole of NH_3 per mole AlN, i.e., 24.4 mmol/g or 546.5 mL/g (based
275 on the H_2 equivalence, this corresponds to 36.6 mmol H_2 /g).

276
277 The regeneration of the nitride may be achieved via the following route:
278
$$\text{Al}_2\text{O}_3 + \text{N}_2 \rightarrow 2\text{AlN} + \frac{3}{2}\text{O}_2 \quad \Delta H^\circ = 1039.7 \text{ kJ/mol} \quad (16)$$

279

280 This highly endothermic reaction is not thermodynamically favorable and the addition of a carbonaceous reducing
281 agent (carbon or methane (Gálvez et al., 2008, 2007b, 2007a)) is necessary according to:

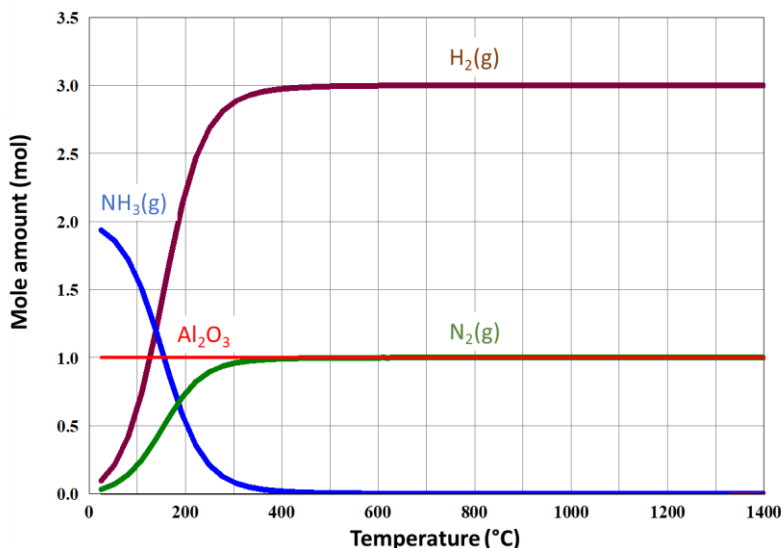
282
$$\text{Al}_2\text{O}_3 + 3\text{C} + \text{N}_2 \rightarrow 2\text{AlN} + 3\text{CO} \quad (17)$$



284
285 The solar-driven carbothermal reduction of Al_2O_3 in N_2 atmosphere has also been studied (Murray et al., 1995).

286
287 Figure 2 shows the equilibrium composition of the $2\text{AlN} + 3\text{H}_2\text{O}$ system (Eq. 15) as a function of temperature at 1
288 bar. The hydrolysis reaction producing ammonia is thermodynamically favorable at low temperature (below
289 $\sim 200^\circ\text{C}$), whereas NH_3 is not stable above 300°C as it decomposes into H_2 and N_2 although a metastable state
290 may exist without the presence of catalysts. It should be noted that similar thermodynamic equilibrium distributions
291 are obtained regardless of the metal nitride considered, with NH_3 being stable only below 300°C .

292



293
294 **Figure 2.** Thermodynamic equilibrium composition of the $2\text{AlN} + 3\text{H}_2\text{O}$ system as a function of the temperature at
295 1 bar.
296

297 A series of ten AlN hydrolysis runs was carried out at temperatures ranging from 200°C to 1200°C . Repeatability
298 of the results was confirmed through different tests with similar conditions. The initial AlN mass did not significantly
299 affect the mass-specific amount of ammonia produced (e.g., 1 mmol/g in run #13 vs. 1.1 mmol/g in run #14 at
300 1000°C). Increasing the temperature was found to significantly improve NH_3 production. Indeed, the NH_3 production
301 rate was low below 1000°C , but it increased drastically above this temperature. This suggests that the reaction is
302 hindered by kinetic limitations since the increase in temperature favors the reaction kinetics, although the reaction
303 is not thermodynamically favorable at high temperatures. Actually, the slow kinetics at low temperatures does not
304 allow thermodynamic equilibrium to be reached in a reasonable reaction time. Figure S1 represents the evolution
305 of the NH_3 production rate at 550°C and 960°C . NH_3 was detected right from the steam was injected, with total
306 production yields (n_{NH_3}) of 0.66 and 0.77 mmol/g, respectively. The NH_3 concentration reached a peak promptly
307 then gradually decreased until reaching negligible values. During AlN sample heating, a weak NH_3 production was
308 measured around 200°C even in the absence of H_2O (Fig. S1b), which suggests a reaction of AlN with residual
309 moisture.

310 Figure 3a shows the evolution of the NH_3 production rates at 1100°C (hydrolysis of 155 mg AlN) and 1200°C
311 (hydrolysis of 156 mg AlN) as a function of time, which confirms the improved kinetics when increasing the
312 temperature. During hydrolysis at 1200°C , the peak production rate of NH_3 reached $1.6 \cdot 10^{-4}$ mol/min/g versus $5 \cdot 10^{-5}$
313 mol/min/g at 1100°C . The total reaction duration decreased from about 40 min at 1100°C to 20 min at 1200°C .
314 Therefore, heating the reactants favored the NH_3 production rate although the reaction was thermodynamically less
315 favorable. The cumulative production of NH_3 reached about 1.1 mmol/g (which corresponds to an NH_3 yield X_{NH_3}
316 of 4.5%). This total NH_3 yield remained almost unchanged whatever the temperature (Fig. 3b). The high
317 temperature necessary to reach a significant hydrolysis rate (above 1000°C) can however represent an obstacle
318 to the implementation of the $\text{Al}_2\text{O}_3/\text{AlN}$ redox system, given that the NH_3 yield is not improved above this
319 temperature.

320

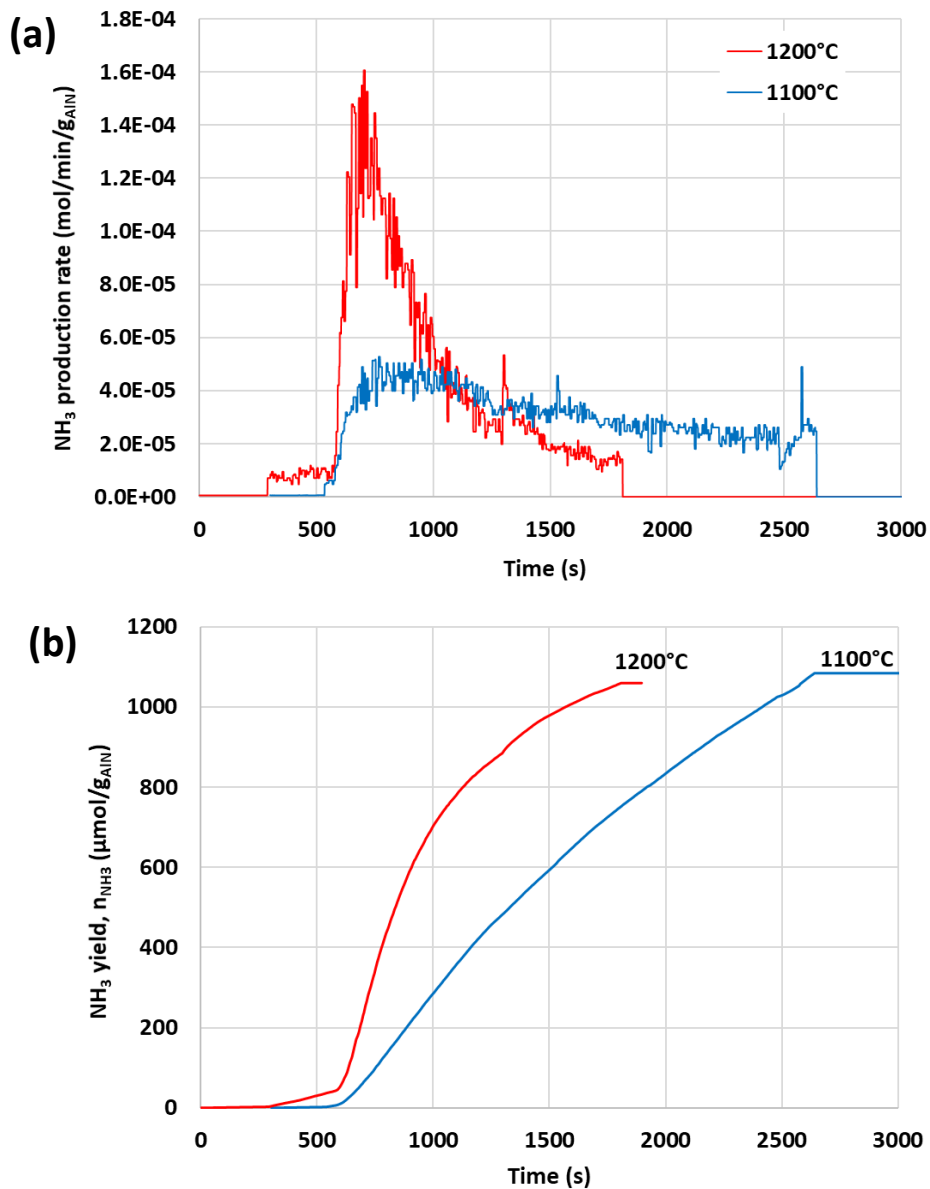


Figure 3. NH_3 production during AlN hydrolysis at 1100°C and 1200°C: (a) evolution of NH_3 production rate as a function of time, (b) cumulative NH_3 production as a function of time.

321
 322
 323
 324
 325
 326
 327
 328
 329
 330
 331
 332
 333
 334
 335

Characterization of the products was carried out to identify the main phases after the hydrolysis reaction and to confirm the oxidation of the nitrides during ammonia synthesis upon exposure to steam. XRD analysis of materials before and after two hydrolysis tests at 1000°C (Fig. 4) showed that the reaction was not complete because AlN was still present in majority after reaction in both tests. In contrast, the products analysis after AlN hydrolysis at 1100°C and 1200°C (Fig. S2) showed that Al_2O_3 was the main species with residual traces of AlN (in lower amount at 1200°C than at 1100°C), which confirmed the efficient conversion of AlN to Al_2O_3 . Some traces of ZrO_2 (tetragonal) were also identified due the zirconia felt used as support for the packed-bed of nitride powder during hydrolysis tests (this support could not be completely eliminated during the recovery of the packed-bed powder after reaction).

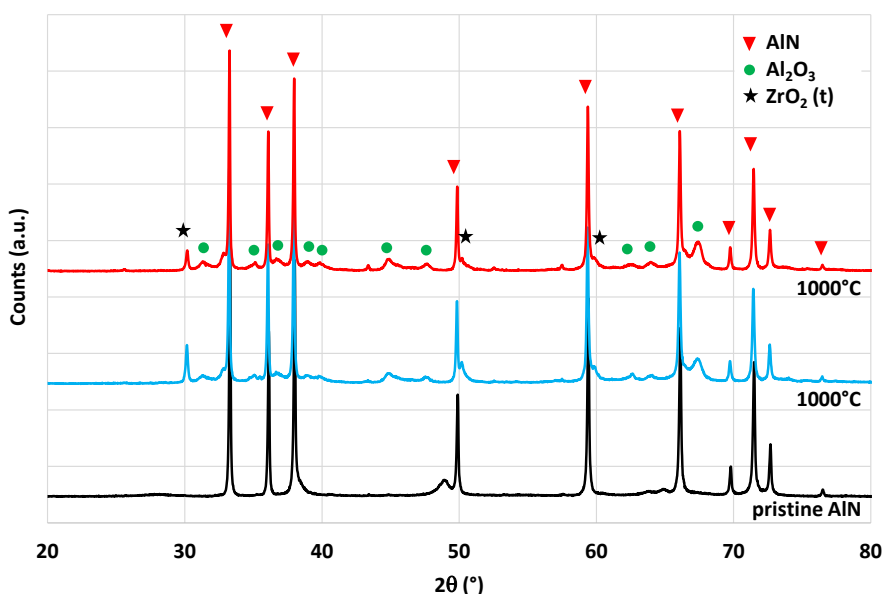


Figure 4. XRD patterns of AlN powders before and after hydrolysis at 1000°C.

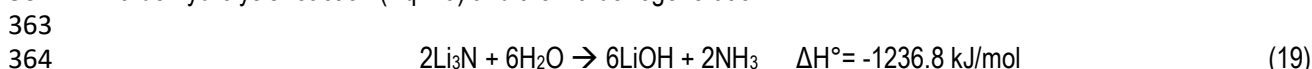
336
337
338

339 A semi-quantitative EDX analysis was carried out for the powders collected after hydrolysis at 1100°C and 1200°C
340 to confirm the complete conversion of the nitride during the reaction. Tables S2-3 report the atomic composition of
341 the powders on different analysis zones (Figs. S3-4). For both temperatures, the Al/O ratio was close to the atomic
342 composition of Al₂O₃ with Al/O = 0.57 at 1100°C and Al/O = 0.69 at 1200°C. The absence of nitrogen (below the
343 detection limit) also denotes that AlN hydrolysis was complete at these temperatures and AlN was efficiently
344 converted to Al₂O₃ after reaction. It should be noted that nitrogen is a light element that is difficult to detect and that
345 it may be present in an amount lower than the detection limit of the analysis method. Figures S5 and S6 show SEM
346 micrographs and X-ray elemental mapping of powders after hydrolysis at 1100°C and 1200°C. The distribution of
347 Al and O is homogeneous, which means that these elements are evenly distributed over the sample surface.
348 Although complete AlN conversion was observed above 1000°C, the NH₃ production yield was low compared to
349 the maximum achievable value from Eq. (15), which is explained by the thermal instability of NH₃. Indeed, ammonia
350 is not stable at high temperatures according to thermodynamics (Figure 2) and can decompose into N₂ and H₂. The
351 NH₃ yield was therefore likely limited by the thermodynamically favorable dissociation of NH₃. These results are
352 consistent with previous kinetic studies performed by thermogravimetric analysis (Gálvez et al., 2007a), in which a
353 reaction conversion close to 95% was reported at 1100°C and 1200°C, and 68% at 950°C using a mixture 80%
354 H₂O-Ar. However, the reaction rate was drastically reduced under 10% H₂O-Ar with a reaction extent of 40% at
355 1200°C after 20 min (complete reaction after ~100 min) and 20% at 1100°C after 30 min. This study also reported
356 a maximum NH₃ yield of 88% obtained at 1000°C for a reaction extent of 93%, which decreased at higher
357 temperatures. Importantly in this study, ammonia was not directly detected and measured by gas analysis, but
358 indirectly quantified by mass balance.

359
360

3.2 Lithium nitride (Li₃N)

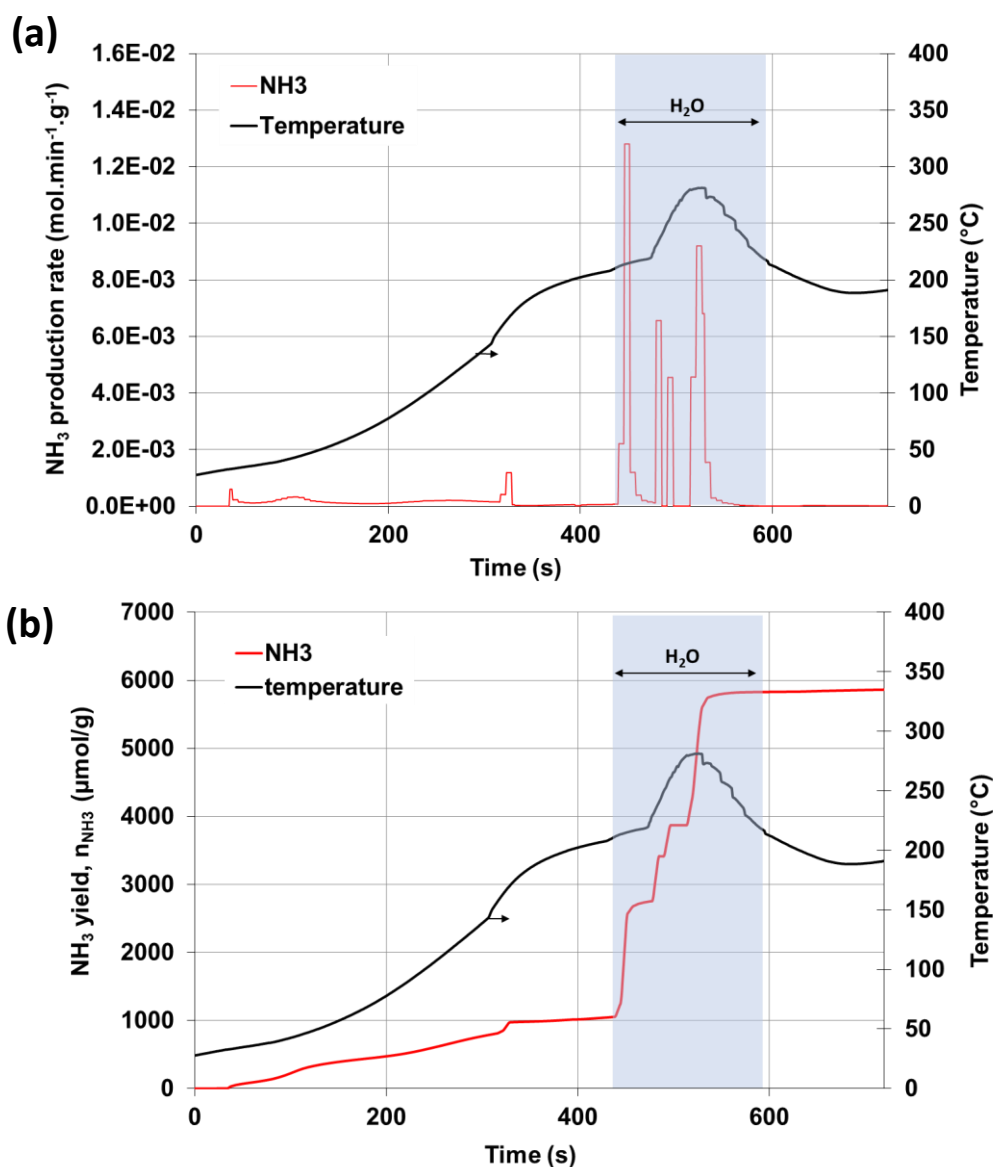
361 The synthesis of ammonia from lithium nitride was considered by Jain et al. (Jain et al., 2017), considering both the
362 nitride hydrolysis reaction (Eq. 19) and the nitride regeneration.



366 The theoretical amount of NH₃ produced corresponds to one mole NH₃ per mole Li₃N, thus 28.7 mmol/g (642.9
367 mL/g) and 43.1 mmol_{H₂}/g relative to the H₂ equivalence. Lithium is a light element, which results in a high mass-
368 specific NH₃ production potential, relative to the mass of material.

369
370 Figure 5a shows the evolution of the NH₃ production rate during Li₃N hydrolysis (107 mg) at 200°C. The reaction
371 rate was fast and several successive peaks in NH₃ production were observed due to unstable steam injection
372 caused by discontinuous droplet feeding. The hydrolysis reaction was completed in less than 2 min. The maximum
373 NH₃ production rate reached 1.28.10⁻² mol/min/g and the total NH₃ yield reached 5.9 mmol/g (Figure 5b),

374 corresponding to a hydrolysis yield of 20.3%. A prompt and substantial increase in temperature (+80°C) was also
 375 observed during the reaction, which can be attributed to the heat generated by the strongly exothermic reaction.
 376 As a result, the product was sintered but could be recovered for solid phase characterization. According to XRD
 377 (Fig. S7), the Li_3N powder was totally converted after hydrolysis with the presence of LiOH phase. These results
 378 are in agreement with previous work on the reaction of lithium nitride with water vapor at 100°C showing major
 379 formation of NH_3 detected by gas chromatography (Jain et al., 2017).
 380



381
 382 **Figure 5.** NH_3 production during Li_3N hydrolysis at 200°C: (a) evolution of NH_3 production rate as a function of
 383 time, (b) cumulative NH_3 production as a function of time.
 384
 385

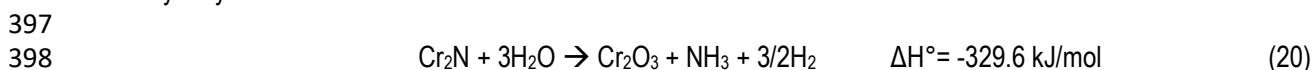
386 3.3 Chromium ($\text{Cr}_2\text{N}/\text{CrN}$), boron (BN), iron (Fe_xN), and silicon (Si_3N_4) nitrides

387 Chromium, iron, boron, and silicon nitrides did not show a high reactivity during hydrolysis regardless of the
 388 temperature considered. Experimental results for the hydrolysis of these nitrides are given in the following without
 389 detailed characterization as they were not identified as suitable candidates for ammonia production.
 390

391 Chromium nitride was previously considered for solar ammonia production (Michalsky and Pfromm, 2011). The
 392 reduction of Cr_2O_3 was carried out in N_2 with the help of a reducing agent such as CO or H_2 , resulting in the formation
 393 of a CrN and Cr_2N mixture. Then, a small amount of NH_3 was measured during hydrolysis in this previous work,

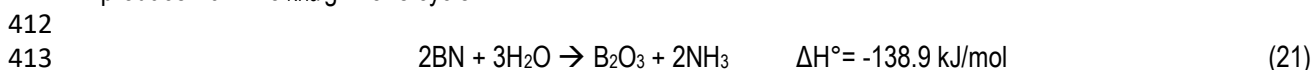
394 which was attributed to the slow corrosion kinetics of this nitride (also well known for its application as a protective
395 coating).

396 The hydrolysis reaction can be written as follows:



399
400 The hydrolysis of commercial chromium nitride (520 mg) composed of a mixture of Cr₂N and CrN phases (Fig. S8,
401 mean Cr/N atomic ratio of 1.7 measured by EDX) was investigated at temperatures of 570°C and 950°C. Figure
402 S9a shows the NH₃ production profile as a function of time with steam injections at 570°C and 950°C. Whatever
403 the temperature, the NH₃ production remained very low with peak production rates of 1.10⁻⁶ mol/min/g and 7.8.10⁻⁶
404 mol/min/g at 570°C and 950°C, respectively. The cumulated value of NH₃ production during CrN hydrolysis was
405 also weak and did not exceed 10 μmol/g (Figure S9b). These results are in agreement with previous studies
406 (1.07×10⁻⁴ mol NH₃/mol Cr/min reported by Michalsky and Pfromm, 2011) and the main reason for this low
407 production was attributed to the preferential formation of N₂ by nitride decomposition instead of NH₃ formation.

408
409 Boron nitride was identified in a theoretical study as a potential candidate material for solar thermochemical NH₃
410 synthesis (Bartel et al., 2019). Equilibrium calculations identified the BN/B₂O₃ redox couple with the ability to
411 produce 10 mmol_{NH₃}/g in one cycle.



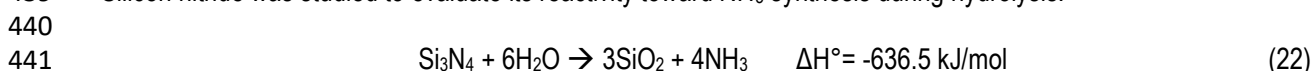
414
415 In order to experimentally test the feasibility of ammonia synthesis, the hydrolysis of commercial boron nitride (198
416 mg) was carried out in this work at different temperatures (pure cubic BN phase was identified by XRD, Fig. S8).
417 Figure S10a shows the NH₃ production profile at 370°C, 700°C, and 970°C. As a result, very weak production rates
418 were observed at the lowest temperatures while a peak production rate of 1.10⁻⁵ mol/min/g was reached at 970°C.
419 However, the cumulated production yield remained low with only 31 μmol_{NH₃}/g (Figure S10b). After the reaction,
420 the material was vaporized and could not be recovered. Therefore, contrary to theoretical predictions, boron nitride
421 did not show suitable hydrolysis reactivity for ammonia synthesis at the different temperatures studied.

422
423 Iron nitride was also previously identified as a potential material for ammonia synthesis (Bartel et al., 2019) and
424 was thus considered in this work. Commercial iron nitride is labeled with a Fe_xN composition (x in the range 2-4).
425 A mean Fe/N atomic ratio of 3.2 was measured by EDX. A phase mixture of mainly Fe₄N with Fe₃N was identified
426 by XRD (Fig. S8).

427 The NH₃ production profile from Fe_xN (400 mg) at 250°C, 550°C, and 1000°C is shown in Figure S11. At 250°C,
428 no production was detected. At 550°C, a peak of NH₃ production was measured with a maximum value at 3.2.10⁻⁴
429 mol/min/g but no further NH₃ was significantly observed at 1000°C. The total cumulative production of NH₃ at 550°C
430 was 230 μmol/g (Figure S11b), which remains well below the theoretically predicted 10 mmol/g. In addition, part of
431 the material was melted and sublimated after the test (rust-colored deposit on the walls of the quartz tube denoting
432 the presence of Fe₂O₃).

433 XRD analysis of the material after hydrolysis was carried out (Figure S12), which revealed the presence of different
434 iron oxide phases (FeO, Fe₂O₃ and Fe₃O₄), without any nitride phase being detected. This shows that NH₃
435 production is not correlated to the oxidation state of the material after hydrolysis. In other words, ammonia formation
436 may not occur even if the material is fully oxidized after hydrolysis. The nitrogen released can indeed form species
437 other than NH₃ (such as N₂) or NH₃ can be thermally decomposed before exiting the reactor.

438
439 Silicon nitride was studied to evaluate its reactivity toward NH₃ synthesis during hydrolysis.



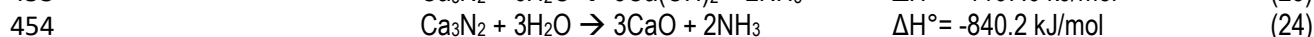
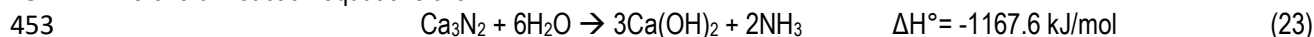
442
443 Figure S13a shows the NH₃ production profile during three consecutive hydrolysis tests of Si₃N₄ (322 mg) at 220°C,
444 520°C, and 980°C. Peaks of NH₃ production rate were observed at the three temperatures and reached 9.10⁻⁶,
445 2.1.10⁻⁴ and 2.6.10⁻⁴ mol/min/g, respectively. The production rate was enhanced when the temperature increased.
446 The cumulative amounts of NH₃ remained low for each temperature and were respectively 5, 65, and 183 μmol/g
447 (Figure S13b). According to XRD (Fig. S14), the Si₃N₄ phase was still the main one detected after hydrolysis,
448 confirming the negligible nitride powder conversion.

449

450 3.4 Calcium nitride (Ca₃N₂)

451 The hydrolysis of calcium nitride has been thoroughly investigated given the good reactivity towards NH₃ synthesis.

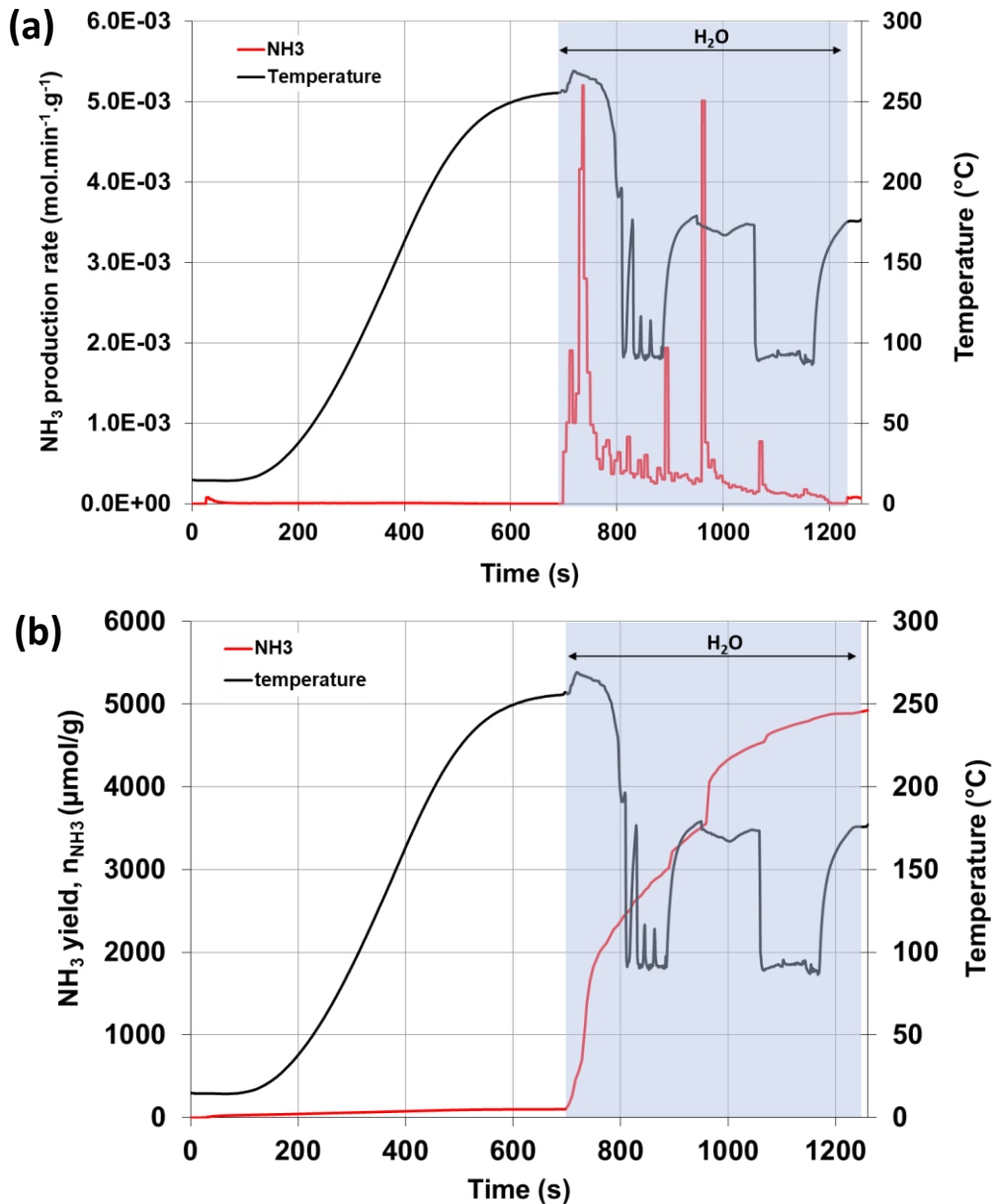
452 The overall reaction equations are:



455

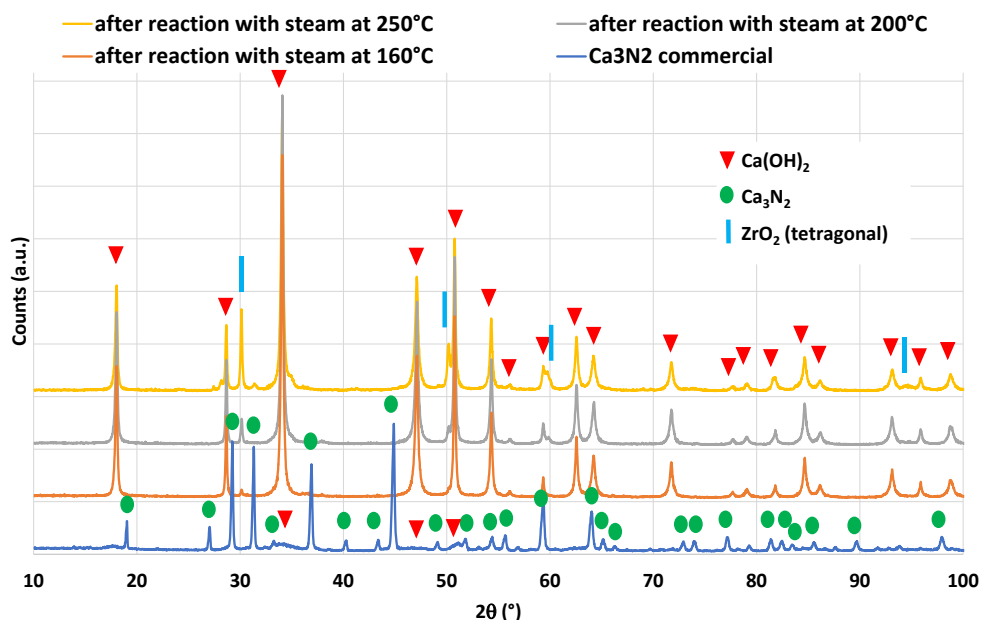
456 Based on Eq. (23), the theoretical maximum NH₃ production is 13.5·10⁻³ mol/g. Figure 6 shows the NH₃ production
457 profile during Ca₃N₂ hydrolysis (100 mg) at 250°C. Calcium nitride is highly reactive during hydrolysis with a peak
458 production rate of NH₃ reaching 5.2·10⁻³ mol/min/g and an overall reaction duration of about 10 min. Steam was
459 injected at a reactor temperature of 250°C inducing a slight temperature increase (260°C) due to the exothermal
460 reaction, but strong temperature variations between 170°C and 90°C were then observed, which can be explained
461 by the energy consumed by the vaporization of water and falling droplets on the thermocouple. Figure 6b plots the
462 cumulative production of NH₃ during Ca₃N₂ hydrolysis, reaching a value of 4.9·10⁻³ mol/g in less than 10 min
463 (corresponding to 36.5% of the theoretical maximum production). The strong temperature drop during hydrolysis
464 (up to ~100°C) may be responsible for the incomplete NH₃ yield. Additional tests were carried out between 170 and
465 290°C and confirmed complete reactions in less than 10 min with an overall NH₃ yield increasing with temperature
466 (~14 mmol/g when the temperature was maintained above 200°C during hydrolysis), as shown in Figure S15. The
467 measured NH₃ production thus corresponds to about 100% of the theoretical maximum production when the
468 temperature is high enough.

469



470
 471 **Figure 6.** NH₃ production during Ca₃N₂ hydrolysis at 260°C: (a) evolution of NH₃ production rate as a function of
 472 time, (b) cumulative NH₃ production as a function of time.

473
 474 The material was characterized by XRD before and after hydrolysis at different temperatures to identify the existing
 475 phases and compare with the fresh material (Figure 7). Whatever the hydrolysis temperature (160°C, 200°C or
 476 250°C), the nitride phase disappeared and Ca(OH)₂ was the main phase identified, which denotes a total oxidation
 477 of the nitride (and a hydration of CaO). A complete conversion of the nitride with water was thus confirmed by XRD.
 478 A tetragonal ZrO₂ phase was also detected, due to zirconia felt as a powder support in the reactor. Also note the
 479 absence of CaO, as calcium hydroxide is stable and does not decompose at these temperatures.
 480



481
482 **Figure 7.** XRD patterns of calcium nitride powders before and after hydrolysis at different temperatures.
483

484 EDX analysis of the powder hydrolyzed at 270°C was carried out. Table S4 reports the atomic composition of the
485 powder, which shows the absence of nitrogen trace in the sample thus confirming the complete nitride conversion.
486 With a composition of 33%_{at} Ca and 65.7%_{at} O, the Ca/O ratio is 0.5, thus corresponding to the atomic ratio in
487 Ca(OH)₂. Traces of zirconium are also detected and correspond to the powder felt support used during the tests.
488 Figure S16 shows the SEM and EDX elemental mapping of the sample composed of Ca and O evenly distributed
489 on the surface.

490 491 **3.5 Magnesium nitride (Mg₃N₂)**

492 The hydrolysis reaction of commercial magnesium nitride (101 mg) was studied, with the following overall
493 equations:



496
497 The calculated maximum NH₃ production is 19.8·10⁻³ mol/g. Figure 8 shows the NH₃ production profile during the
498 hydrolysis of Mg₃N₂ at 190°C. During steam injection, the temperature dropped rapidly due to water vaporization.
499 A substantial production of NH₃ was measured with a maximum peak rate of 1.8·10⁻² mol/min/g and an overall
500 reaction duration of less than 10 min, as confirmed by the NH₃ production returning to zero before the end of steam
501 injection. The cumulative production of NH₃ during Mg₃N₂ hydrolysis at 190°C was 18.6·10⁻³ mol/g (Figure 8b),
502 which corresponds to 94% of the maximum theoretical NH₃ yield.

503 Other tests were also carried out at slightly different temperatures (from 120 to 275°C) and confirmed the
504 repeatability of the results with complete conversion achieved after about 5 to 10 min of hydrolysis reaction.
505

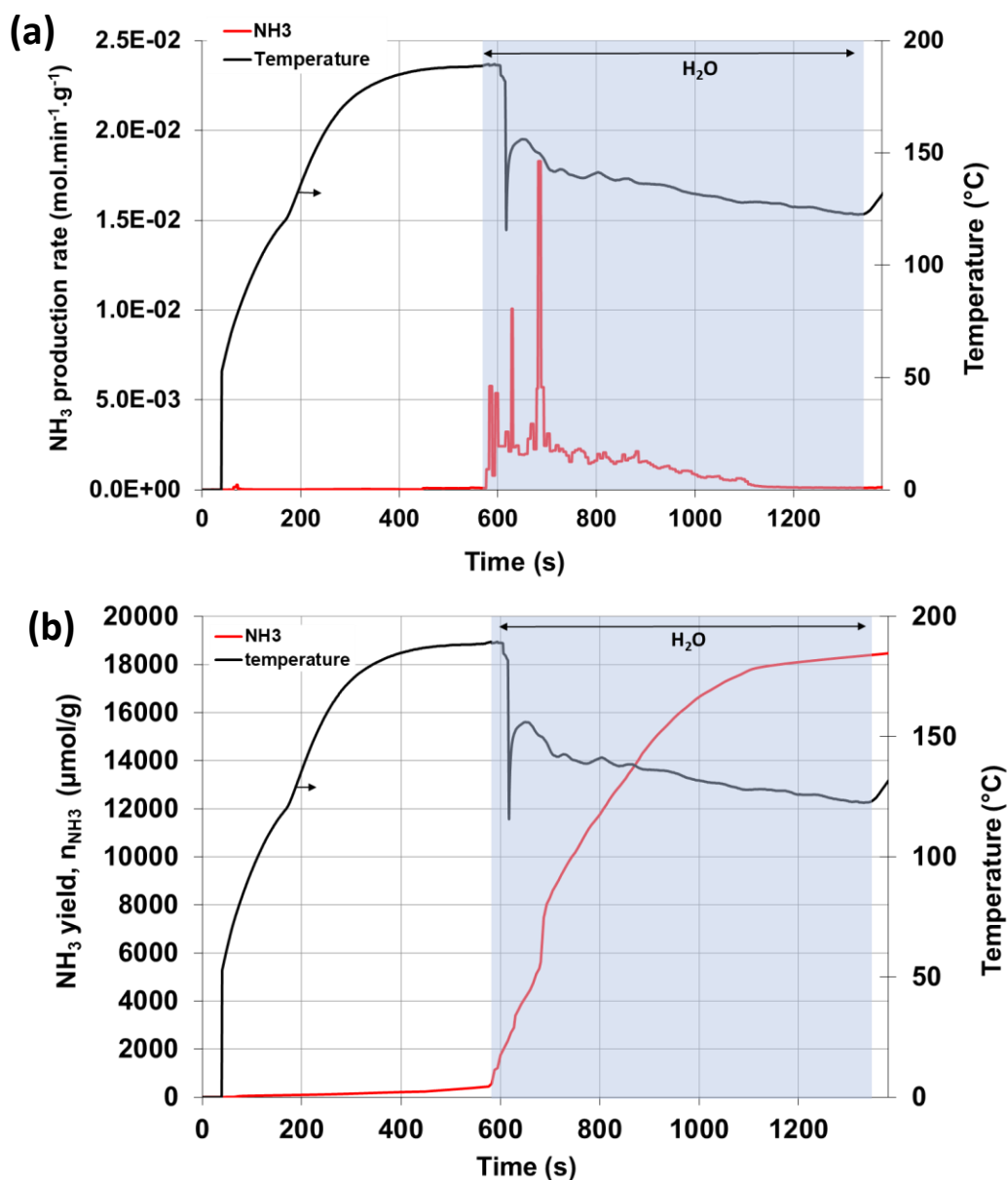


Figure 8. NH₃ production during Mg₃N₂ hydrolysis at 190°C: (a) evolution of NH₃ production rate as a function of time, (b) cumulative NH₃ production as a function of time.

506
507
508
509
510
511
512
513
514
515
516

The magnesium nitride powder was characterized by XRD before and after hydrolysis at different temperatures in order to identify the main phases after reaction and to compare them with the pristine material (Figure 9). The nitride phase completely disappeared after reaction whatever the temperature (200°C or 270°C) and both MgO and Mg(OH)₂ were formed, which demonstrates the complete nitride conversion. The peaks related to MgO were higher than those related to Mg(OH)₂ at the highest temperature, which highlights the decomposition of Mg(OH)₂ to MgO with increasing temperature. Some ZrO₂ (tetragonal) from the felt support was also detected, as already mentioned previously for the other materials.

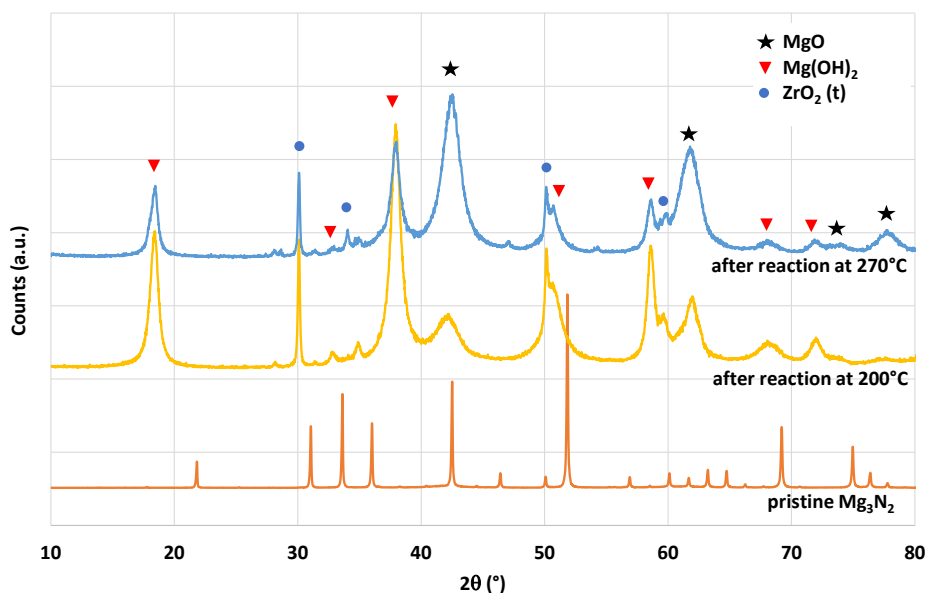


Figure 9. XRD patterns of magnesium nitride powders before and after hydrolysis at different temperatures.

517
518
519

EDX analysis of the powder hydrolyzed at 270°C was performed and the atomic composition is reported in Table S5. No trace of nitrogen was detected, which confirms the complete nitride conversion. With a composition of 35.3%_{at} Mg and 61.6%_{at} O, the Mg/O ratio is 0.57, corresponding to an intermediate ratio between MgO and Mg(OH)₂ in agreement with the results of XRD analysis. Traces of zirconium are also detected corresponding to the felt support.

Figure S17 shows SEM and EDX elemental mapping related to the atomic composition of the sample. The powder is composed of Mg and O evenly distributed over the surface.

525
526
527

3.6 Titanium nitride (TiN)

Titanium nitride was considered for solar production of NH₃, with the following hydrolysis reaction equation:

529
530



531
532

Titanium can also form oxy-nitride species of varying composition and stoichiometry, which can impact the overall equation. Based on Eq. (27), the theoretical maximum production of NH₃ is 16.1·10⁻³ mol/g. According to thermodynamics (Fig. S18), the formation of NH₃ is only predicted below 300°C because it decomposes at higher temperatures, and secondary oxide and oxy-nitride minor phases are predicted at higher temperatures (above ~800°C).

Figure 10a shows the evolution of the NH₃ production rate during TiN hydrolysis at 900°C, 970°C, and 1000°C. Although the reaction was not thermodynamically favored at high temperatures, the peak production rate increased with increasing temperature due to a kinetically-controlled reaction. The NH₃ production rate rose from 2.4·10⁻⁴ mol/min/g at 900°C, to 3.4·10⁻³ mol/min/g at 1000°C. The reaction duration was short whatever the temperature since NH₃ production was completed in less than ~3-4 min, indicating fast kinetics. Other hydrolysis reactions carried out at 250°C and 500°C did not produce NH₃, which means that the temperature must be high enough to obtain noticeable kinetics. Figure 10b shows the cumulative production of NH₃ during TiN hydrolysis at different temperatures. The NH₃ production increased significantly with temperature as it was 2.16 mmol/g at 900°C, 3.06 mmol/g at 970°C, and 4.05 mmol/g at 1000°C.

543
544
545
546
547

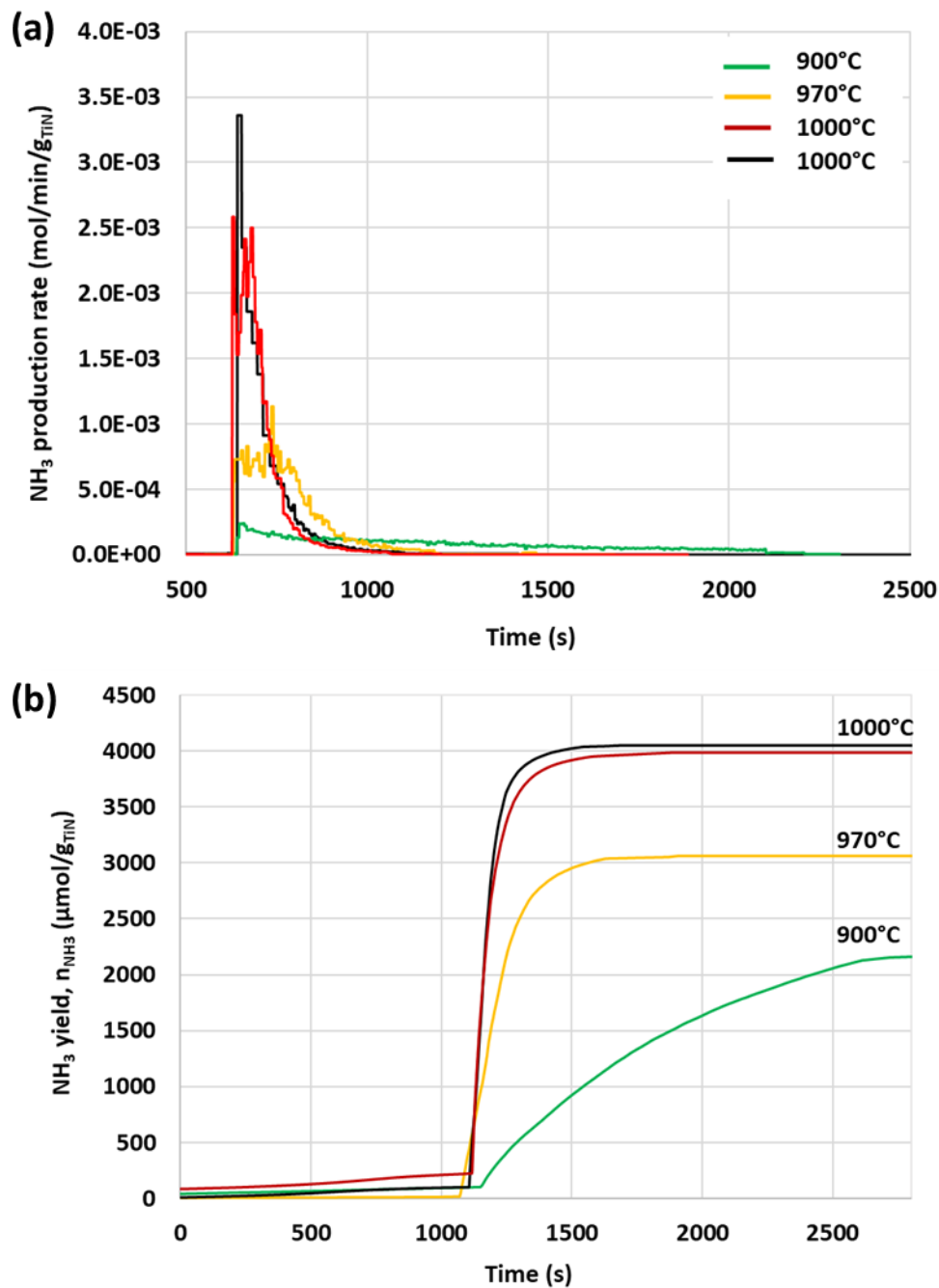
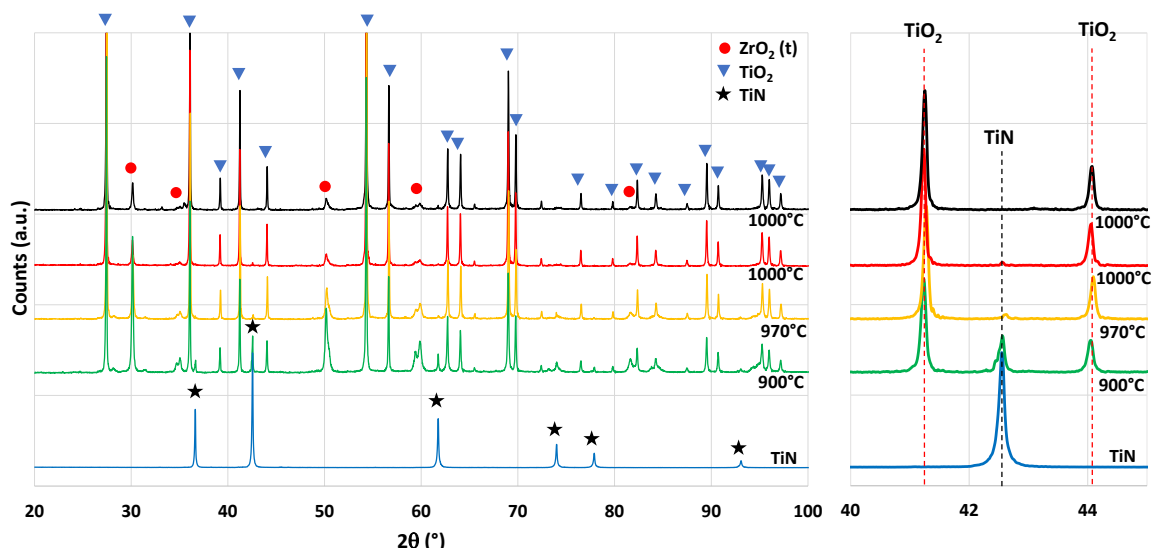


Figure 10. NH_3 production during TiN hydrolysis at 900°C, 970°C and 1000°C: (a) evolution of NH_3 production rate as a function of time, (b) cumulative NH_3 production as a function of time.

548
549
550
551
552
553
554
555
556
557

XRD analysis of titanium nitride powders before and after hydrolysis at different temperatures was carried out (Figure 11). TiO_2 (rutile) was observed as the main phase after hydrolysis at each temperature considered. The initial TiN phase was still detected at 900°C but remained in very low amount. The intensity of TiN peaks relative to TiO_2 decreased when temperature increased, confirming an improvement in reaction extent. $\text{ZrO}_2(\text{t})$ from the felt support was also detected, consistently with previous results.



558
559 **Figure 11.** XRD patterns of TiN powders before and after hydrolysis at different temperatures.
560

561 EDX analysis of TiN powders hydrolyzed at 900°C, 970°C, and 1000°C was performed and Table S6 reports the
562 atomic compositions. The Ti/O ratio is 0.52 at 1000°C, corresponding approximately to TiO₂ composition. No trace
563 of nitrogen was detected at any hydrolysis temperature, which means it is below the detection limit. The traces of
564 zirconium correspond to the felt support.

565 Figures S19-S21 show the SEM and EDX elemental mapping of powders hydrolyzed at 900, 930 and 1000°C,
566 confirming the homogeneous distribution of the Ti and O elements.
567

568 3.7 Zirconium nitride (ZrN)

569 The final material tested in this study of nitride hydrolysis for NH₃ production was zirconium nitride (ZrN).
570



572
573 As for Ti, Zr can form oxy-nitrides which can modify the overall equation of the reaction. Based on Eq. (28), the
574 theoretical maximum production of NH₃ is $11.0 \cdot 10^{-3}$ mol/g.

575 The NH₃ production profiles during ZrN hydrolysis were studied at 550°C, 620°C, 750°C, 820°C, 920°C, and
576 1000°C (Figures 12 and S22). An increase in the peak production rate was measured until it reached an optimum
577 at 750°C and decreased at higher temperatures (Table 1). The maximum NH₃ production rate at 750°C reached
578 34.2 mmol/min/g (767 mL/min/g), which was the highest reaction rate obtained among the nitrides tested. The
579 period of NH₃ production was short, as the reaction was completed in less than about 2-3 min, except at the lowest
580 temperature of 550°C where the kinetics were much slower. Figure 12b reports the cumulative production of NH₃
581 during ZrN hydrolysis at different temperatures, with an optimum at 750°C corresponding to a maximum NH₃
582 production yield of 12.3 mmol/g (Fig. S23).
583

584 **Table 1.** Peak production rates and yields of NH₃ during ZrN hydrolysis at different temperatures.

	Peak production rate (mmol/min/g)	Peak production rate (mL/min/g)	Yield of NH ₃ (mmol/g)
550°C	0.50	11.3	7.9
620°C	17.6	393.4	11.4
750°C	34.2	767.0	12.3
820°C	21.8	488.9	11.2
920°C	25.1	562.2	8.3
1000°C	15.7	352.9	2.1
1010°C	1.16	26.0	0.75

585
586
587

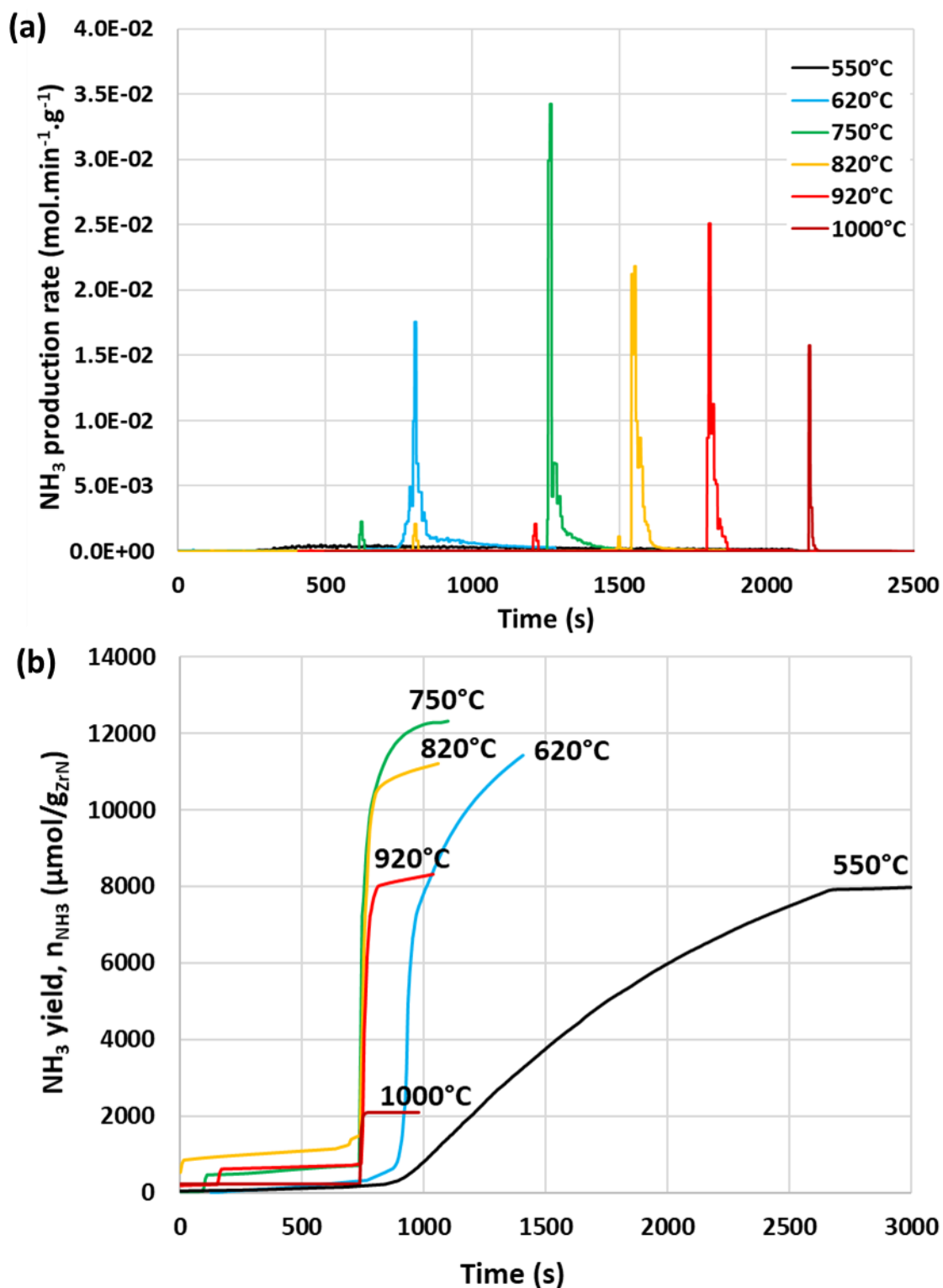


Figure 12. NH_3 production during ZrN hydrolysis at different temperatures: (a) comparison of NH_3 production rate, (b) cumulative NH_3 production as a function of time.

589
590
591
592
593
594
595
596
597

XRD analysis of zirconium nitride powders before and after hydrolysis at different temperatures (Figure 13) shows that ZrO_2 (monoclinic and tetragonal) is the main phase after the reaction at any temperature. The intensity ratio of peaks related to monoclinic ZrO_2 increases with temperature. The initial ZrN phase is still observed especially at 550°C and 620°C, and it disappears at higher temperatures, which confirms the enhanced hydrolysis extent when increasing the temperature.

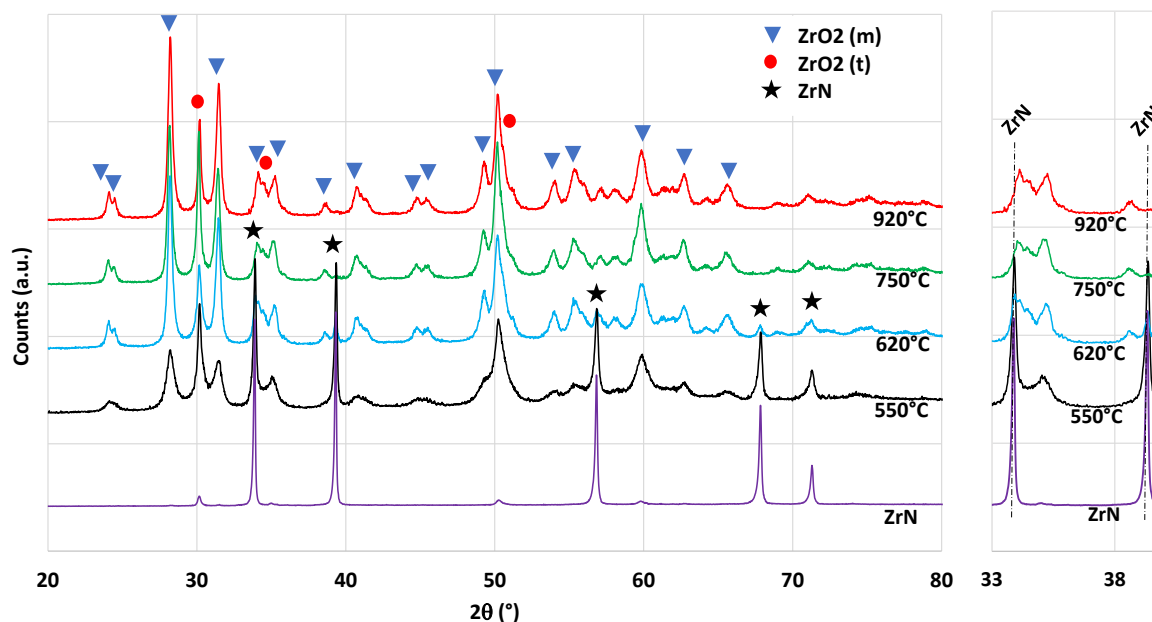


Figure 13. XRD patterns of ZrN powders before and after hydrolysis at different temperatures.

598
599
600
601
602
603
604
605
606
607
608
609

EDX analysis of powders hydrolyzed at 620°C, 750°C, 820°C, and 920°C was performed and Table S7 reports the atomic composition, confirming the overall ZrO₂ composition after hydrolysis (Zr/O ratio of ~0.5). Some nitrogen was always detected, except for the powder hydrolyzed at 750°C, in agreement with the maximum conversion observed at this temperature.

Figures S24-S27 show the SEM and EDX elemental mapping of powders hydrolyzed at 620, 750, 820, and 920°C. A homogeneous distribution of Zr, O and N is evidenced.

This study successfully demonstrated the production of ammonia from the hydrolysis of ZrN with fast rates and optimum conversion at 750°C. The next step will focus on the solar regeneration of nitrides from ZrO₂ oxide.

4. Conclusion

610
611
612
613
614
615
616
617
618
619
620
621
622
623
624
625
626
627
628
629
630
631
632
633
634

The production of ammonia via two-step cycles relying on N₂ and H₂O as the only feedstocks is an attractive approach, as it uses solar heat as the process energy input and additionally bypasses the use of H₂. Active materials involved in such thermochemical cycles (metal oxide/nitride redox pairs) must be identified and optimized to demonstrate the feasibility of the solar ammonia production process. A series of ten metal nitrides was experimentally tested for ammonia production from nitrides hydrolysis. Iron (FeN), chromium (CrN), boron (BN), and silicon (Si₃N₄) nitrides gave no significant NH₃ production, and therefore cannot be considered as suitable candidate materials for thermochemical ammonia production cycles. Among the considered nitrides, the most attractive materials turned out to be AlN, Li₃N, Ca₃N₂, Mg₃N₂, TiN, and ZrN because they exhibit a noteworthy reactivity during hydrolysis and a significant production of NH₃. The influence of temperature was studied for each material and proved to have a strong impact on the reaction conversion and the NH₃ yield. AlN hydrolysis occurred significantly above 1000°C with maximum rates at 1200°C (0.16 mmol/min/g), but the NH₃ yield remained moderate (1.1 mmol/g) presumably due to decomposition at high temperatures. TiN and ZrN also required high temperatures for NH₃ production. A maximum NH₃ production rate of 3.4 mmol/min/g was measured at 1000°C for TiN (NH₃ yield of 4.1 mmol/g), while an optimum temperature of 750°C was revealed for ZrN yielding the highest NH₃ production rate of 34.2 mmol/min/g (NH₃ yield of 12.3 mmol/g). The hydrolysis reactions of Li₃N, Ca₃N₂, and Mg₃N₂ were the most exothermic and thus required low temperatures (around 200°C) to achieve complete conversion, with total NH₃ yields of 5.9, 4.9, and 18.6 mmol/g, respectively. The hydrolysis rate of Ca₃N₂ and Mg₃N₂ was slightly lower than that of Li₃N, TiN, and ZrN.

This study thus demonstrated the feasibility of sustainable ammonia synthesis from a novel clean process ultimately based on concentrated solar energy as the process heat source. Noteworthy ammonia production performance was achieved with the identified metal nitrides. Thermochemical ammonia production based on nitrides cycles is a suitable means for industrial process decarbonation. Future work will focus on the regeneration step of the metal nitrides using concentrated solar energy at high temperatures. The most reactive nitrides were found to be Li₃N,

635 Ca₃N₂, Mg₃N₂, TiN and ZrN. The solar-driven nitridation reaction of the corresponding oxides (Li₂O, CaO, MgO,
636 TiO₂, and ZrO₂) must therefore be characterized as a function of temperature and reducing agent to demonstrate
637 the complete cycles of nitride chemical looping for ammonia synthesis.
638

639 **Declaration of Competing Interest**

640 The authors declare that they have no known competing financial interests or personal relationships that could
641 have appeared to influence the work reported in this paper.
642

643 **Acknowledgments**

644 This work was partially funded by the CNRS Energy Unit (Cellule Energie) through the PEPS AMMOSOL project.
645 The authors acknowledge the support from the PCM characterization platform (E. Bêche) at PROMES-CNRS
646 during the XRD analysis.
647

648 **Appendix A. Supplementary material**

649 The following is the Supplementary material related to this article.
650

651 Supplementary material contains a summary of the experimental conditions and the corresponding total amounts
652 of NH₃ produced during the different hydrolysis tests, additional NH₃ production data for metal nitrides hydrolysis,
653 materials characterization including XRD analysis data and SEM/EDX imaging/elemental mapping.
654

655 **Data availability**

656 Data will be made available on request.
657

658

659 **References**

- 660
- 661 Abanades, S., 2023. A Review of Oxygen Carrier Materials and Related Thermochemical Redox Processes for
662 Concentrating Solar Thermal Applications. *Materials* 16, 3582. <https://doi.org/10.3390/ma16093582>
- 663 Abanades, S., 2022. Redox Cycles, Active Materials, and Reactors Applied to Water and Carbon Dioxide Splitting
664 for Solar Thermochemical Fuel Production: A Review. *Energies* 15, 7061.
665 <https://doi.org/10.3390/en15197061>
- 666 Aziz, M., Wijayanta, A.T., Nandiyanto, A.B.D., 2020. Ammonia as Effective Hydrogen Storage: A Review on
667 Production, Storage and Utilization. *Energies* 13, 3062. <https://doi.org/10.3390/en13123062>
- 668 Bartel, C.J., Rumptz, J.R., Weimer, A.W., Holder, A.M., Musgrave, C.B., 2019. High-Throughput Equilibrium
669 Analysis of Active Materials for Solar Thermochemical Ammonia Synthesis. *ACS Appl. Mater. Interfaces*
670 11, 24850–24858. <https://doi.org/10.1021/acsami.9b01242>
- 671 Bhaskar, A., Assadi, M., Nikpey Somehsaraei, H., 2020. Decarbonization of the Iron and Steel Industry with
672 Direct Reduction of Iron Ore with Green Hydrogen. *Energies* 13, 758.
673 <https://doi.org/10.3390/en13030758>
- 674 Ceballos, B.M., Pilia, G., Ramaiyan, K.P., Banerjee, A., Kreller, C., Mukundan, R., 2021. Roads less traveled:
675 Nitrogen reduction reaction catalyst design strategies for improved selectivity. *Current Opinion in*
676 *Electrochemistry* 28, 100723. <https://doi.org/10.1016/j.coelec.2021.100723>
- 677 Chambon, M., Abanades, S., Flamant, G., 2010a. Solar thermal reduction of ZnO and SnO₂: Characterization of
678 the recombination reaction with O₂. *Chemical Engineering Science* 65, 3671–3680.
679 <https://doi.org/10.1016/j.ces.2010.03.005>
- 680 Chambon, M., Abanades, S., Flamant, G., 2010b. Design of a Lab-Scale Rotary Cavity-Type Solar Reactor for
681 Continuous Thermal Dissociation of Volatile Oxides Under Reduced Pressure. *Journal of Solar Energy*
682 *Engineering* 132, 021006. <https://doi.org/10.1115/1.4001147>
- 683 Chuayboon, S., Abanades, S., 2019. Clean magnesium production using concentrated solar heat in a high-
684 temperature cavity-type thermochemical reactor. *Journal of Cleaner Production* 232, 784–795.
685 <https://doi.org/10.1016/j.jclepro.2019.05.371>
- 686 Daisley, A., Hargreaves, J.S.J., 2023. Metal nitrides, the Mars-van Krevelen mechanism and heterogeneously
687 catalysed ammonia synthesis. *Catalysis Today* 423, 113874.
688 <https://doi.org/10.1016/j.cattod.2022.08.016>

689 Damanabi, A.T., Servatan, M., Mazinani, S., Olabi, A.G., Zhang, Z., 2019. Potential of tri-reforming process and
690 membrane technology for improving ammonia production and CO₂ reduction. *Science of The Total*
691 *Environment* 664, 567–575. <https://doi.org/10.1016/j.scitotenv.2019.01.391>

692 Gálvez, M.E., Frei, A., Halmann, M., Steinfeld, A., 2007a. Ammonia Production via a Two-Step Al₂O₃/AlN
693 Thermochemical Cycle. 2. Kinetic Analysis. *Ind. Eng. Chem. Res.* 46, 2047–2053.
694 <https://doi.org/10.1021/ie061551m>

695 Gálvez, M.E., Halmann, M., Steinfeld, A., 2007b. Ammonia Production via a Two-Step Al₂O₃/AlN Thermochemical
696 Cycle. 1. Thermodynamic, Environmental, and Economic Analyses. *Ind. Eng. Chem. Res.* 46, 2042–
697 2046. <https://doi.org/10.1021/ie061550u>

698 Gálvez, M.E., Hischer, I., Frei, A., Steinfeld, A., 2008. Ammonia Production via a Two-Step Al₂O₃/AlN
699 Thermochemical Cycle. 3. Influence of the Carbon Reducing Agent and Cyclability. *Ind. Eng. Chem.*
700 *Res.* 47, 2231–2237. <https://doi.org/10.1021/ie071244w>

701 Goto, Y., Daisley, A., Hargreaves, J.S.J., 2021. Towards anti-perovskite nitrides as potential nitrogen storage
702 materials for chemical looping ammonia production: Reduction of Co₃ZnN, Ni₃ZnN, Co₃InN and Ni₃InN
703 under hydrogen. *Catalysis Today* 364, 196–201. <https://doi.org/10.1016/j.cattod.2020.03.022>

704 Haeussler, A., Abanades, S., Jouannaux, J., Drobek, M., Ayrál, A., Julbe, A., 2019. Recent progress on ceria
705 doping and shaping strategies for solar thermochemical water and CO₂ splitting cycles. *AIMS Materials*
706 *Science* 6, 657–684. <https://doi.org/10.3934/mat.2019.5.657>

707 Hunter, S.M., McKay, D., Smith, R.I., Hargreaves, J.S.J., Gregory, D.H., 2010. Topotactic Nitrogen Transfer:
708 Structural Transformation in Cobalt Molybdenum Nitrides. *Chem. Mater.* 22, 2898–2907.
709 <https://doi.org/10.1021/cm100208a>

710 Jain, A., Miyaoka, H., Kumar, S., Ichikawa, T., Kojima, Y., 2017. A new synthesis route of ammonia production
711 through hydrolysis of metal – Nitrides. *International Journal of Hydrogen Energy* 42, 24897–24903.
712 <https://doi.org/10.1016/j.ijhydene.2017.08.027>

713 Kishira, S., Qing, G., Suzu, S., Kikuchi, R., Takagaki, A., Oyama, S.T., 2017. Ammonia synthesis at intermediate
714 temperatures in solid-state electrochemical cells using cesium hydrogen phosphate based electrolytes
715 and noble metal catalysts. *International Journal of Hydrogen Energy* 42, 26843–26854.
716 <https://doi.org/10.1016/j.ijhydene.2017.09.052>

717 Klaas, L., Guban, D., Roeb, M., Sattler, C., 2021. Recent progress towards solar energy integration into low-
718 pressure green ammonia production technologies. *International Journal of Hydrogen Energy* 46, 25121–
719 25136. <https://doi.org/10.1016/j.ijhydene.2021.05.063>

720 Kyriakou, V., Garagounis, I., Vasileiou, E., Vourros, A., Stoukides, M., 2017. Progress in the Electrochemical
721 Synthesis of Ammonia. *Catalysis Today* 286, 2–13. <https://doi.org/10.1016/j.cattod.2016.06.014>

722 Laassiri, S., Zeinalipour-Yazdi, C.D., Catlow, C.R.A., Hargreaves, J.S.J., 2018. The potential of manganese
723 nitride based materials as nitrogen transfer reagents for nitrogen chemical looping. *Applied Catalysis B:*
724 *Environmental* 223, 60–66. <https://doi.org/10.1016/j.apcatb.2017.04.073>

725 Lai, Q., Cai, T., Tsang, S.C.E., Chen, X., Ye, R., Xu, Z., Argyle, M.D., Ding, D., Chen, Y., Wang, J., Russell, A.G.,
726 Wu, Y., Liu, J., Fan, M., 2022. Chemical looping based ammonia production—A promising pathway for
727 production of the noncarbon fuel. *Science Bulletin* 67, 2124–2138.
728 <https://doi.org/10.1016/j.scib.2022.09.013>

729 Le Gal, A., Abanades, S., 2011. Catalytic investigation of ceria-zirconia solid solutions for solar hydrogen
730 production. *International Journal of Hydrogen Energy* 36, 4739–4748.
731 <https://doi.org/10.1016/j.ijhydene.2011.01.078>

732 Liu, X., Elgowainy, A., Wang, M., 2020. Life cycle energy use and greenhouse gas emissions of ammonia
733 production from renewable resources and industrial by-products. *Green Chem.* 22, 5751–5761.
734 <https://doi.org/10.1039/D0GC02301A>

735 Marnellos, G., Stoukides, M., 1998. Ammonia Synthesis at Atmospheric Pressure. *Science* 282, 98–100.
736 <https://doi.org/10.1126/science.282.5386.98>

737 Marnellos, G., Zisekas, S., Stoukides, M., 2000. Synthesis of Ammonia at Atmospheric Pressure with the Use of
738 Solid State Proton Conductors. *Journal of Catalysis* 193, 80–87. <https://doi.org/10.1006/jcat.2000.2877>

739 Michalsky, R., Avram, A.M., Peterson, B.A., Pfromm, P.H., Peterson, A.A., 2015a. Chemical looping of metal
740 nitride catalysts: low-pressure ammonia synthesis for energy storage. *Chem. Sci.* 6, 3965–3974.
741 <https://doi.org/10.1039/C5SC00789E>

742 Michalsky, R., Parman, B.J., Amanor-Boadu, V., Pfromm, P.H., 2012. Solar thermochemical production of
743 ammonia from water, air and sunlight: Thermodynamic and economic analyses. *Energy* 42, 251–260.
744 <https://doi.org/10.1016/j.energy.2012.03.062>

745 Michalsky, R., Pfromm, P.H., 2011. Chromium as reactant for solar thermochemical synthesis of ammonia from
746 steam, nitrogen, and biomass at atmospheric pressure. *Solar Energy* 85, 2642–2654.
747 <https://doi.org/10.1016/j.solener.2011.08.005>

748 Michalsky, R., Pfromm, P.H., Steinfeld, A., 2015b. Rational design of metal nitride redox materials for solar-driven
749 ammonia synthesis. *Interface Focus* 5, 20140084. <https://doi.org/10.1098/rsfs.2014.0084>

750 Michalsky, R., Steinfeld, A., 2017. Computational screening of perovskite redox materials for solar
751 thermochemical ammonia synthesis from N₂ and H₂O. *Catalysis Today* 286, 124–130.
752 <https://doi.org/10.1016/j.cattod.2016.09.023>

753 Mordor Intelligence LLP, 2021. Ammonia Market - Growth, Trends, COVID-19 Impact, and Forecasts (2021 -
754 2026) (No. 6036753).

755 Murakami, T., Nishikiori, T., Nohira, T., Ito, Y., 2003. Electrolytic Synthesis of Ammonia in Molten Salts under
756 Atmospheric Pressure. *J. Am. Chem. Soc.* 125, 334–335. <https://doi.org/10.1021/ja028891t>

757 Murakami, T., Nohira, T., Ogata, Y.H., Ito, Y., 2005a. Electrolytic Ammonia Synthesis in Molten Salts under
758 Atmospheric Pressure Using Methane as a Hydrogen Source. *Electrochem. Solid-State Lett.* 8, D12.
759 <https://doi.org/10.1149/1.1870633>

760 Murakami, T., Nohira, T., Ogata, Y.H., Ito, Y., 2005b. Electrochemical Synthesis of Ammonia and Coproduction of
761 Metal Sulfides from Hydrogen Sulfide and Nitrogen under Atmospheric Pressure. *J. Electrochem. Soc.*
762 152, D109. <https://doi.org/10.1149/1.1904984>

763 Murray, J., Steinfeld, A., Fletcher, E., 1995. Metals, nitrides, and carbides via solar carbothermal reduction of metal
764 oxides. *Energy* 20, 695–704. [https://doi.org/10.1016/0360-5442\(95\)00032-C](https://doi.org/10.1016/0360-5442(95)00032-C)

765 Patisson, F., Mirgautx, O., 2020. Hydrogen Ironmaking: How It Works. *Metals* 10, 922.
766 <https://doi.org/10.3390/met10070922>

767 Qing, G., Kikuchi, R., Kishira, S., Takagaki, A., Sugawara, T., Oyama, S.T., 2016. Ammonia Synthesis by N₂ and
768 Steam Electrolysis in Solid-State Cells at 220°C and Atmospheric Pressure. *J. Electrochem. Soc.* 163,
769 E282–E287. <https://doi.org/10.1149/2.0161610jes>

770 Rafiqul, I., Weber, C., Lehmann, B., Voss, A., 2005. Energy efficiency improvements in ammonia production—
771 perspectives and uncertainties. *Energy* 30, 2487–2504. <https://doi.org/10.1016/j.energy.2004.12.004>

772 Wang, L., Xia, M., Wang, H., Huang, K., Qian, C., Maravelias, C.T., Ozin, G.A., 2018. Greening Ammonia toward
773 the Solar Ammonia Refinery. *Joule* 2, 1055–1074. <https://doi.org/10.1016/j.joule.2018.04.017>

774 Xiao, L., Wu, S.-Y., Li, Y.-R., 2012. Advances in solar hydrogen production via two-step water-splitting
775 thermochemical cycles based on metal redox reactions. *Renewable Energy* 41, 1–12.
776 <https://doi.org/10.1016/j.renene.2011.11.023>

777 Yang, S., Zhang, T., Yang, Y., Wang, B., Li, J., Gong, Z., Yao, Z., Du, W., Liu, S., Yu, Z., 2022. Molybdenum-
778 based nitrogen carrier for ammonia production via a chemical looping route. *Applied Catalysis B:
779 Environmental* 312, 121404. <https://doi.org/10.1016/j.apcatb.2022.121404>

780
781